DETERMINATION OF SUBSURFACE STORMFLOW USING TRACER METHOD

by

ADARSH S S

(2017-18-008)

Department of Soil and Water Conservation Engineering

KELAPPAJI COLLEGE OF AGRICULTURAL ENGINEERING AND TECHNOLOGY

TAVANUR-679573, MALAPPURAM

KERALA, INDIA

2020

DETERMINATION OF SUBSURFACE STORMFLOW USING TRACER METHOD

By

ADARSH S S

(2017-18-008)

Thesis

Submitted in partial fulfillment of the requirement for the degree of

Master of Technology

In

Agricultural Engineering

(Soil and Water Engineering)

Faculty of Agricultural Engineering and Technology

Kerala Agricultural University

Department of Soil and Water Conservation Engineering

KELAPPAJI COLLEGE OF AGRICULTURAL ENGINEERING AND TECHNOLOGY

TAVANUR-679573, MALAPPURAM

KERALA, INDIA

2020

DECLARATION

I, hereby declare that this thesis entitled **''DETERMINATION OF SUBSURFACE STORMFLOW USING TRACER METHOD"** is a bonafide record of research work done by me during the course of research and the thesis has not previously formed the basis for the award to me of any degree, diploma, associateship, fellowship or other similar title of any other University or Society.

Tavanur **ADARSH S S**

10/02/2020 **(2017-18-008)**

CERTIFICATE

Certified that this thesis entitled **"DETERMINATION OF SUBSURFACE STORMFLOW USING TRACER METHOD"** is a record of research work done independently by Mr. Adarsh S S (2017-18-008) under my guidance and supervision and that it has not previously formed the basis for the award of any degree, diploma, fellowship or associateship to him.

Dr. Sathian K. K.
(Major Advisor, Advisory Committee)
Professor and Head
Department of Soil and Water Conservation Engineering
Kelappaji College of Agricultural Engineering and Technology
Tavanur.

Tavanur

10/02/2020

CERTIFICATE

We, the undersigned members of the advisory committee of Adarsh S S (2017-18-007), a candidate for the degree of **Master of Technology in Agricultural Engineering** with major in Soil and Water Engineering, agree that the thesis entitled **"DETERMINATION OF SUBSURFACE STORMFLOW USING TRACER METHOD"** may be submitted by Adarsh S S (2017-18-008), in partial fulfilment of the requirement for the degree.

Dr. Sathian K. K.
(Major Advisor, Advisory Committee)
Professor and Head
Dept. of SWCE
KCAET, Tavanur.

Dr. Abdul Hakkim V. M.
Professor
College of Agriculture
Padanakkad.

Er. Shivaji K. P.
Asst. Professor
Dept. of FMPE
KCAET, Tavanur.

Dr. Jinu A.
Asst. Professor
Dept. of SWCE
KCAET, Tavanur

ACKNOWLEDGMENT

ACKNOWLEDGMENT

With whole heartedness I thank '**God the Almighty**' for the help, rendered through various hands, which helped me to the completion of this endeavor.

None other than my guide **Dr. Sathian K. K.,** *Professor and Head*, Dept. of SWCE, KCAET, Tavanur deserves at the second place, my heartfelt thanks for his persistent initiation, efficacious advice and zealous intellectual support.

I am greatly indebted to **Dr. Abdul Hakkim V. M.**, *Professor,* College of Agriculture, Padanakkad for his interest and kind advice given to me at all stages of my studies.

I express my heartfelt thanks to **Er. Shivaji. K.P**. *Assistant Professor,* Dept. of FPME, KCAET Tavanur, for his valuable suggestions and motivation.

I place my special thanks to**, Dr. Jinu A**., *Assistant Professor*, Dept. of SWCE his suggestions and invaluable help during my study.

I would like to place my special thanks to **Dr. Reshmi T. R.**, *Head i/c & Scientist*, Isotope Hydrology Division, CWRDM, Kerala for her priceless guidance and suggestions.

I would like to place my special thanks to my senior **Er. Jyothy Narayanan,** for her sincere help and support during my research.

I would also like to thank my junior **Mr. Rolvin Presanna Pera** for his immense contribution for completing my research.

Words do not suffice to express my gratitude to all my **seniors**, **classmates and friends** who have helped me immensely during the period of my study and the research work.

I am thankful to all the **department staffs and faculties** of KCAET, Tavanur for their cooperation and kind advices.

I express my thanks to all the staff members of **library, KCAET Tavanur** for their ever willing help and co-operation.

I am greatly indebted to my **parents** for their blessings and prayers and support without which I could not have completed this work.

I am thankful to **all those**, who directly or indirectly helped me.

ADARSH S S

DEDICATED TO

THE PROFESSION OF AGRICULTURAL ENGINEERING ...

CONTENTS

LIST OF TABLES

LIST OF FIGURES

LIST OF PLATES

SYMBOLS AND ABBREVIATIONS

Symbols	Abbreviations
%	Percent
cm	Centimeter
Dept.	Department
DF	Degrees of freedom
dS m^{-1}	Deci siemens per meter
EC	Electrical conductivity
Er.	Engineer
et al.	and others
etc	et cetera
Fig.	Figure
FMPE	Farm Machinery and Power Engineering
SWCE	Soil and Water Conservation Engineering
g	Gram
h	hour(s)
i.e.	that is
KAU	Kerala Agricultural University
KCAET	Kelappaji College of Agricultural Engineering and Technology
l	Liter
M	Meter(s)
kPa	Kilo Pascal
l m^{-2} day^{-1}	Liter per meter squared per day
cm day^{-1}	Centimeter per day

INTRODUCTION

CHAPTER I

INTRODUCTION

Water is considered as the most vital natural resource required for the survival of all the living organisms. So, all water resources should be managed precisely and judiciously. Unfortunately, scarcity of water can be felt all over the world, even in places with an abundance of annual precipitation. The state of Kerala is a typical example of a region or state in India facing droughts of varying degrees despite receiving high magnitude of annual rainfall. The state faces acute water shortage for various purposes including drinking during non-rainy seasons. This is because the groundwater potential of the terrain is not in accordance with the high rainfall magnitude and high infiltration rate of the topsoil. Therefore, it is to be inferred that a large portion of the infiltrated water is escaped from the vadose zone (root zone) region quickly after rainfall events.

The traditional hydrology suggests the flow of precipitated water on earth be of two types. They are surface flow and subsurface flow. Subsurface flow refers to any flow below the surface of the ground which may contribute to interflow, baseflow or percolation (WMO, 2012). The subsurface flow can be divided into quick flow and low flow components. The quick flow refers to subsurface stormflow and the low flow refers to base flow. The quick flow is a mechanism that produces runoff mostly operating in upland terrains. Subsurface stormflow contributes to storm hydrograph in a river. It occurs when water moves laterally through soil layers or permeable bedrock. Subsurface stormflow could be treated as the main process of storm runoff generation in the steep terrains having a humid environment with permeable soils (Anderson and Burt, 1990). Subsurface stormflow only occurs in lowlands with gentle topography and dry climate at extreme conditions like high rainfall and high antecedent soil moisture so that momentary water tables form and pressurize lateral flow towards streams. In the hydrological literature, the term subsurface stormflow is also substituted as subsurface runoff, throughflow, lateral flow, interflow, transient groundwater, fast subsurface flow or soil water flow. Being an important process of subsurface flow, subsurface stormflow mainly describes

the process that generates runoff and releases into the transient, near-channel wetlands that develop during the storm event and enters the channel without meeting the groundwater zone. Even though it has a drainage capacity slower than the overland flow, it is faster than the groundwater flow. It is responsible for quickly responding of the streamflow during a storm event. So it can cause surprising fast drainage of soils and conveys water to contribute to storm flow.

All the processes that generate runoff and occurs on subsurface but near the soil surface which will result in a stream channel hydrograph response at the time of a precipitation event could be subsurface stormflow. These processes occurring below the soil surface may be coupled directly to flow in preferential pathways like soil pipes or interconnected macropores and layers or areas having high conductivity. The regimes of flow in subsurface soil may be divided into homogeneous matrix flow (uniform flow) and preferential flow (nonuniform flow) (Weiler et al., 2003). Both often occur concurrently but have significantly different consequences for water flow as well as chemical leaching. The homogeneous matrix lateral flow can be a feasible stormflow process if the water is already collected in soil, within the connected saturated or close-to-saturated areas. In slopes having a high permeable soil layer with a high infiltration capacity above a low permeable soil layer often results in a big contribution of pre-event water to the streams. While the preferential lateral flow happens either in characteristic structures in the soil where the water flow is only due to gravity (macropores) or in areas having a greater permeability than the adjacent soil matrix. Soil macropores or bedrock fractures which are aligned parallel to the slope may convey water competently and rapidly from hillslope to the stream (Beven and Germann, 1982). The forest areas where macropores are produced by plant roots or burrowing animals are generally dominated by preferential through laterally oriented macropores. The term soil pipe is used for the interconnected macropores that are broadened by erosion and lengthened over several meters (Anderson and Burt, 1990). If the disconnected macropores are getting connected hydraulically during storms, it can also cause effective drainage of the hillslopes (Weiler et al., 2003).

Mainly in the steep and humid catchments, the subsurface stormflow is

considered to be omnipresent. However, due to spatial heterogeneity as well as the spatial and temporal variation in the precipitation circulation, the transport activity of subsurface stormflow is very much convoluted. Even in the case of small catchments or hillslopes, the origin and passage of subsurface stormflow are often found to be different. The occurrence and strength of subsurface stormflow are generally affected by the following factors.

- Amount, intensity, and duration of rainfall
- Texture, thickness, structure, antecedent moisture of the soil
- Biological characteristics such as vegetation cover, plant root, animal burrow, and land use patterns
- Topographic factors such as slope, surface, and subsurface topography
- Land use patterns.

Literature survey suggests that there is very little information on the subsurface hydrologic processes with regard to their spatial and temporal movement. It is postulated that the groundwater recharge of an area having a high infiltration rate such as the lateritic terrain of midlands of Kerala is adversely affected by the subsurface storm flow. It decreases the quantity and opportunity time of percolation water to the water table or groundwater storage. In sloping terrains with high permeability, lateral flow is reported to be very considerable (Sathian and Syamala, 2009). It is again assumed that the fast component of lateral flow known as subsurface storm flow is the main factor adversely affecting the quantum of percolation. At the same time, detailed knowledge on the process of subsurface flow phenomenon is not available Therefore, a quantitative analysis of subsurface stormflow is very much essential to plan appropriate water conservation interventions.

The early studies of subsurface flow used trenches (or pits) combined with hydrometric approaches for its observation. Subsurface stormflow is not only a major contributor to the volume of flow to the streams, but it is also accountable for the conveyance of some nutrients into surface water bodies. So the chemistry of the

water discharging into the streams could be used for tracing out the source areas of subsurface stormflow. The same technique could be used to trace out the pathways of flow with the application of artificial tracers. With the application of tracer hydrology and geophysical techniques great evolution has been made on the source, pathway, and residence time of subsurface flow. However, there is no broad development in the field that explains the detailed mechanism responsible for the process of subsurface stormflow.

With better knowledge on subsurface storm flow phenomenon, it would be possible to suggest more effective measures for augmenting percolation to groundwater and thereby increasing the stored groundwater potential. In this context, this study has been envisioned to throw more insight into the phenomenon of subsurface stormflow with the following objectives.

1. To quantify the quick component of lateral flow (subsurface storm flow) in typical lateritic slopes.
2. To analyse the spatial and temporal movement of subsurface stormflow within the vadose zone profile of the soil.

REVIEW OF LITERATURE

CHAPTER II

REVIEW OF LITERATURE

2.1 HISTORY AND EVOLUTION OF SUBSURFACE STORMFLOW

The evolution of the knowledge on the processes of the conversion of rainfall to streamflow and runoff generation has started slowly since Horton (1933) discovered the relationship between infiltration and overland flow from his study on the role of infiltration in the hydrologic cycle. It is known as Horton's infiltration theory of surface runoff. He assumed that the infiltration will occur uniformly throughout the watershed. He proposed that during the event of rainfall the infiltration ability decreases until the intensity of the rainfall event increases to initiate the surface runoff. This excess rainfall was thought to produce the overland flow throughout the catchment at once. And thus it was proposed that only this overland flow generates the stormflow.

While Horton's infiltration theory was one extreme of the spectrum, the other extreme was identified by Hursh (1936) as the subsurface stormflow. In the hydrological literature, this subsurface stormflow is also depicted as interflow, lateral flow or subsurface runoff.

Hursh and Brater (1941) quantified the role of subsurface stormflow in an experimental catchment in the forested Coweeta experimental watershed, North Carolina. For their study, they have used the records from 40 acres of drainage area and analysed a large number of storm hydrographs. From this experiment, they inferred that the stream hydrograph response to storm rainfall at the experimental watershed comprises of two constituents. One is the channel precipitation while the other one is the subsurface stormflow.

Later Hoover and Hursh (1943), through their study on influence of soil depth on runoff from a forested land in Coweeta experimental watershed, North Carolina with the analysis of drainage area data and storm hydrographs indicated that the components such as depth of soil, topography of the watershed and the connected hydrologic traits of different elevations will affect the peak discharge.

The perception rate on the context of subsurface stormflow was progressing throughout the International Hydrological Decade (IHD). The major work during this frame of time was done by Hewlett and Hibbert (1963). They studied the energy and moisture conditions within the soil mass of 40 % slope and a bulk density of 1.3 g cm^{-3} in order to give a proper explanation about the source of the nonstorm streamflow occurring in deep-soiled areas in the southern Appalachians, United States. For their study, they have constructed a 3×3×45 foot inclining concrete trough of 40 % slope. The structure was then packed with natural sandy loam soil to attain a bulk density of 1.3 g cm^{-3}. After a thorough soaking, the structure was covered to eliminate evaporation losses. The outflow at the base, soil moisture tension and soil moisture content were observed for 145 days. The soil moisture tension and soil moisture content studies supported the theory that the entire soil mass was contributing to outflow throughout the experiment. Based on the study they stated that the subsurface flow through the earth mantle of watersheds having steep slope cannot be overlooked in hydrograph analysis.

Hewlett and Hibbert (1967) conducted a study on the aspects which will affect the precipitation responses of small catchments in humid areas within 20 square miles. They separated long term hydrograph records from fifteen forested watersheds from the eastern United States into quick and delayed flow by computer and then ranked according to the mean precipitation, quick flow and response factor quick flow/precipitation and quick flow/total water yield. Then they compared similar data from nine agricultural watersheds with twenty-four small basins. This indicated that the factors average soil mantle depth, average land slope, the average number of large storms and land use will largely determine the response of small watersheds to storms within the humid region.

Singh and Callaghan (1978) studied the effect of interflow on soil drainage with a sand tank model. Their study included the comparison of different drainage configurations on the rate of removal of water in steady state and on the rate of drawdown of the water table in the non-steady state. Their study concluded that the long term rate of lowering of the water table is mainly due to the hydraulic

conductivity of the lower layer soil. When the water table is high, a good amount of horizontal flow takes place in the permeable top layer.

The first detailed study on subsurface stormflow at the "Maimai" watershed in New Zealand was done by Mosely (1979). The study area was located in one of the eight experimental watersheds in Tiwhai State forest, New Zealand. The gross precipitation was measured using a Lambrecht recording rain gauge. The through fall through the canopy of forest was caught with the help of a 90 m of 10 cm wide plastic guttering which leads to connected drums. The water level in the drum was measured by a Belfort FW1 water level recorder. The runoff from the watershed was measured using a 90^{o} V-notch equipped with water level recorder. The study revealed a close relation in the time of peaks of subsurface stormflow and discharge peaks in the streams. The suggested flow was in the form of a saturated wedge. It was also found that the rate of water movement through the soil could be up to 300 times the soil saturated hydraulic conductivity.

Ahuja and Ross (1983) conducted a theoretical study on the effect of subsoil conductivity and thickness on interflow pathways, rates and source areas for chemicals in a sloping and layered soil with seepage face. They have inferred that the subsurface storm flow characteristics are able to predict from the known parameters with the help of some simplified approaches. The study also showed how the pathways, source areas and rates of interflow are affected by the relative conductivity and thickness of subsoil and the leakiness of base.

Sklash *et al.* (1986) followed the studies at Maimai watershed, New Zealand. They used hydrometric observations and analysed the samples from rainfall, soil water, and streamflow for chloride, electrical conductivity, deuterium, and oxygen-18 composition for natural tracer studies in two first order and one second order streams and in six throughflow pits for evaluating the roles of old and new water during three storm events in September 1983. With this analysis, they understood that the major mixing of the old and new water is occurring at the hillslope and the subsurface flow towards the stream was found to be an isotopically uniform mixture of stored water.

Mc Donnel (1990) studied the old water discharge through macropores in steep humid catchments in Maimai catchments, New Zealand. He monitored continuous energy conditions in two discrete catchment positions for a series of storm events in 1987. He related the tensiometric responses to the soil water characteristic curve, hillslope throughflow, and total catchment runoff. This study depicted that macropore flow or preferential flow can result in old water transportation.

Mc Donnel *et al.* (1991) used the technique of combining chemical and isotope tracing with the tensiometric data. They monitored a 97 m^2 zero-order basin within the 3.8 ha Maimai 8 catchment situated in West cost of New Zealand and studied the soil water potentials, slope throughflow, runoff chemistry and isotopic composition for a natural rain storm and two artificial rain applications. It was found that the endurance of water table at the boundary of soil and bedrock was very short and in these zones, the interconnection of soil pipes was large enough to account for sudden watertable depletion and decline of pore water pressure.

Freer *et al.* (2002) studied about the function of the bedrock topography on subsurface stormflow by conducting an elaborate study of subsurface flow and water table response incorporated with digital terrain analysis (DTA) of both surface and subsurface features at the hillslope scale in Panola Mountain Research Watershed (PMRW), Georgia. They excavated a 20 m long and 15 m wide artificial trench to bedrock along the lower boundary of the hillslope site. This area was then covered using a roofing structure and sidewalls were made to eliminate direct rainfall to the trench area. The trench was instrumented with tipping bucket and all the water from the tipping bucket was directed towards downslope to drain into the 30 m slope area before the stream. The trenched area was also instrumented with tensiometers. The study clearly established that rather than the surface topography, the local bedrock topography plays a significant role in the subsurface runoff at the hillslope scale in the catchments where the bedrock surface performs as a comparatively impermeable boundary.

Sathian and Syamala (2009) worked on the calibration and validation of a physically-based distributed watershed hydrological model, SWAT. They applied the model to Kunthipuzha sub-basin of Bharathapuzha river basin in Kerala. The daily rainfall data of seven years (1996 to 2002) is used for the simulation of the model and the validation of its prediction accuracy was done using daily observed river flow. The results of their study indicated that the lateral flow component as a percentage of annual rainfall is 22 %.

According to the International Glossary of Hydrology by WMO (2012), subsurface flow can be defined as any flow occurring below the surface of the ground which may contribute to interflow, base flow or percolation.

In the study done by Bosch., *et al*., (2017) on temporal variations in baseflow for the Liittle River experimental watershed in South Georgia, USA, the separation of stream flow is considered as subjective since there is no method for separately identifying them. So they divided the streamflow into two components, stormflow and baseflow. Stormflow contains the surface runoff and the quickflow portion of the subsurface storm flow while baseflow contains groundwater flow and the portion of subsurface storm flow moving slowly through subsoil contains groundwater flow and the portion of subsurface storm flow moving slowly through subsoil.

2.2 FLOW REGIMES

2.2.1 Homogeneous Matrix Flow

The homogeneous matrix lateral flow can be an unavoidable portion in subsurface stormflow if the soil matrix is already saturated. In slopes having a high permeable soil layer with a high infiltration capacity above a low permeable soil layer often results in a big contribution of pre-event water to the streams. In the modern approach, the soil is considered as a dual-porosity media termed as microporosity and macroporosity. The movement of water through smaller pores is assumed to be uniform or otherwise negligible. This microporosity, which is also termed as the matrix porosity, corresponds to uniform matrix flow. Skopp (1981)

gave the definition to matrix porosity as the soil volume which will carry solutes and water gently enough to ensure diffusion as well as dispersion between pores.

Mosley (1982) studied the subsurface flow through soils in Tawhai, Big Bush and Craigeieburn State Forests, New Zealand. He studied the process by applying water to a line source 1 m upslope from a pit so that the subsurface flow will intercept at the trough located in the base of the line source. He observed the lag times between the centres of mass of input and outflow between the start of input and start of outflow. He replicated the same experiments for 51 locations. The mean and maximum velocities of flow were found to be 0.3 cm s^{-1} and 0.42 cm s^{-1} respectively. He observed that moderate storms develop saturated wedge which reach the soil surface on lower slopes because of which the velocities found were high.

The theoretical study was done by Rawls *et al.* (1993) for predicting the saturated hydraulic conductivity with the help of fractal principles. The study aimed for developing the equations that are capable of predicting both matrix and macropore saturated conductivity and to relate the parameters in the equation to the soil properties which are readily available. The equation for the prediction of matrix and macropore saturated hydraulic conductivity were developed by coupling fractal process with the Marshall saturated conductivity formulation. The equations were developed with the use of matrix porosity, macropore porosity, maximum pore radius and number of pore classes. They developed the predicting equations by relating the number of pore classes and maximum pore radius to soil properties. They modified the Marshall saturated hydraulic conductivity equation which is able to provide a reasonable approximation of matrix and macropore saturated hydraulic conductivity. The equation is also applicable to a wide range of soil textures,

The process of stormflow is described as the lateral flow at the soil-bedrock interface in the study done by Tani (1997) for estimating the runoff generation processes on a steep hill slope with a thin layer of soil. The study was carried out in order to obtain a better understanding the runoff generation processes on a forested hillslope having large heterogeneities. The study was conducted in

Tatsunokuchi-yama Experimental Forest in the Forestry and Forest Products Research Institute (FFPRI), Japan. The effects of forest changes with respect to streamflow have been studied in two of the adjacent catchments for more than 58 years from 1937. The runoff from each catchment were monitored using 60^{o} V-notch. Other climatic factors were measured at an observation station. From this study, he found that almost all the rainfall contributes to storm runoff when the soil condition is wettest. The application of a kinematic wave runoff model revealed that a quick lateral flow receiving a quick propagation of rainfall pulse storm runoff in the wettest stage. He observed no response in a very dry condition which is due to non-existence of wet zones near to the stream.

2.2.2 Preferential flow

German and Beven (1981) approached the process of flow of water through macropores experimentally to estimate the volume of macropore system and its effect on the infiltration capacity with a soil water potential concept. They investigated the macropore systems of two large and undisturbed soil samples. The volume of macropore systems were found to be 0.01 and 0.045 of the sample volumes respectively. They noted that when the samples were drained from saturation to a point of complete drain of water, the hydraulic conductivity decreased by factors of 18 and 4.3 respectively.

Beven and Germann (1981) studied the process of water transportation through the soil macropores for demonstrating the influence of macropores on the rate of infiltration through soils having different hydraulic conductivities. They investigated the macropore systems of two large and undisturbed soil samples. They presented a one dimensional model of bulk flow in a combined micropore/macropore system. The model has developed by the results obtained from the experimental setup of samples. The results of several simulations by the model demonstrated the effect of macropores on infiltration rates in soils of different hydraulic conductivity.

Then Beven and Germann (1982) reviewed the importance of macropores in water flow through the soil and concluded that the macropores will efficiently and rapidly transport water in soil or fractures in bedrock positions parallel to the slope. They have also concluded that the interconnected macropores which are formed by roots, animals, soil structure or cracks can influence the drainage as well as infiltration in well-structured soil significantly.

Anderson and Burt (1990) reviewed the knowledge of subsurface flow process of their time. They examined the models used for the prediction of contributing areas to storm runoff. They termed the developed macropores due to erosion, which are connected over several meters as “soil pipes”.

Kumar *et al.* (1997) conducted field experiments at the Agricultural Engineering and Agronomy Research Centre (AEARC), Iowa, United States for the study on the separation of matrix and preferential flows with the use of tile flow data. Six subsurface tiles, each draining an area of 0.4 ha were observed. Deep sumps were installed to intercept the tile lines. Continuous record of the tile flow rates as a function of time were made. The study results concluded that, for all rainfall events, preferential flow contributes about 13 % of the total subsurface tile outflow and a contribution of 10-20 % annually.

The understanding of the important regimes of runoff and solute transport at the hillslope scale has remained a major unsolved topic for researchers. Weiler *et al.* (2003) conducted the research on controls of macropore connectivity over water flow and solute transport in the hillslopes of Maimai, New Zealand and Fudoji, Japan. They used a physically based hillslope model HILL-VI for the comparative study with field experimental data. With this study they pointed that the hillslope soils with high drainable porosity are less influenced by lateral pipeflow. Their study also revealed that the peak runoff is strongly influenced by pipe flow as the runoff reduces 30 % of observed when the pipe flow is not taken into account.

A detailed review on soil piping was done by Richards and Reddy (2007) related to earth dam construction, the field in which piping was determined as an important process. They defined the major types of piping as:

1. Eluviation: washing out of materials in mass leaving behind a loose mass of granular materials which is vulnerable to collapse.
2. Clay soil dispersion by rainfall.
3. Backward erosion of materials through pipe openings from springs.
4. Erosion occurring along antecedent openings.

Oberdorster *et al.* (2016) investigated the preferential flow processes in a forest soil using time domain reflectometry and electrical resistivity tomography during a saline tracer experiment. The investigated site is located on the premises of the Julich Research Centre, Germany. The field plot was equipped with 36 ERT boreholes to monitor the natural changes in the soil water content. The peak velocities of preferential flow at different depths showed an increasing character as going deeper. They also found a rapid increase in peak velocity of preferential flow between 84 cm and 124 cm depths. This acceleration coincided with a strong decrease in the electrical conductivity change. This result suggested that it is caused due to the considerable decrease in the effective pore volume through the traces travelled.

2.3 MEASUREMENT APPROACHES

2.3.1 Trenching

Trenching is the physically-based direct field study together with hydrometric data for subsurface stormflow research as well as hillslope investigation. Whipkey (1965) made a trench and trough system for water seepage up to 150 cm and studied the subsurface stormflow from a forested slope in Allegheny Plateau, Ohio, United States. The study site was of 28 % slope and had sandy loam soil. Rainfall was simulated using rainstorms with intensity of 1.7 to 5.1 cm h^{-1}. He got a significant quantity of outflow from 0 to 56 cm depth having sandy loam soil.

A much advanced use of trenches was done by Freer *et al.* (2002) on experimental hill slopes. He studied the functions of bedrock topography on subsurface stormflow Panola Mountain Research Watershed, Georgia. Artificial trench of 20 m long and 1.5 m wide was excavated to bedrock along the hill slope lower boundary. This area was covered with roofing to prevent direct runoff to the trench. The subsurface flow through the trench was collected for 10 separate 2 m sections for the whole soil profile using tipping bucket and CR10 data logger. Times of initial rise varied from 512 h to 648. The majority of the trench section was characterized by the middle and deeper section (4-16 m), 16-20 m section gave much more rapid times to peak and recession responses and 0-4 m right side of the trench has lower responses.

Most of the subsurface stormflow investigations using trenching approach have examined only a few numbers of storm events. So Tromp-van Meerveld and McDonnell (2006a) have done the subsurface stormflow response analysis for 147 storm events at the trenches hillslopes of Panola Mountain Research Watershed, Georgia. They have used a long term data set for the analysis of threshold relations in subsurface stormflow. They found a clear threshold response of subsurface stormflow to the total storm precipitation as 55 mm. For the events exceeding the threshold, there was a magnitude increase in the order of 2 compared to the storms smaller than the threshold. They have also observed a linear relationship between the total pipe flow and the total subsurface stormflow.

Tromp-van Meerveld and McDonnell (2006b) also investigated the processes which caused the threshold responses. For that, they installed maximum rise crest gauges in a dense array manner and recording wells on the hillslope, Panola Mountain Research Watershed, Georgia and analysed the spatial as well as the temporal variation of transient saturation at the interface of the bedrock. They found that when the rainfall reaches above 55 mm, the depressions on the hillslope will get filled and the subsurface saturated region become connected to the trench. From that instant, the subsurface stormflow rate increases more than five folds than before. The total subsurface stormflow was also 75 times more than before. This

showed that the microtopography influences the connectivity of saturated subsurface areas to slope-scale and the contribution of hillslope to flow at the catchment scale.

Graham *et al.* (2010) done a combined study of irrigation and excavation experiment at the well-studied Maimai hillslope, New Zealand having an area of 0.5 ha for achieving new insights on how the various source areas and pathways are formed and connects the rainfall to the downstream flow across the hillslope. They performed two sets of irrigation experiments above the trench section. The first experiment was the subsurface injection of water and tracer 8 m upslope of trench sections. The second one was the line source surface application of water and tracer 4 m upslope of another trench section. The study results showed that with wet antecedent moisture conditions and large rainfall amount the near-surface layer of 10 cm soil profile contributes 37 % to 62 % to storm runoff. However, with dry antecedent conditions, the deeper subsurface layers significantly contribute 33 % to 71 % to the total hillslope discharge. So, with increasing the subsurface saturation, the vertical percolation decreases and lateral flow increasingly occur at top layers instead of deeper layers. Their findings suggested that the subsurface flow path controlling factors were microscale bedrock topography, bedrock permeability and lateral subsurface velocities rather than the surface topography.

2.3.2 Tracer Method

The era of tracer hydrology started about years ago and developed slowly but fascinatingly. Hewlett and Hibbert (1967) studied the factors affecting precipitation responses of small catchments in the humid areas. For their study they separated long term hydrograph records in eastern United States into quick and delayed flow by computer and ranked them according to the mean precipitation, quick flow and response factor quick flow/precipitation and quick flow/total water yield. Then they compared similar data from nine agricultural watersheds with twenty-four small basins. This indicated that the factors average soil mantle depth, average land slope, the average number of large storms and land use will largely determine the response of small watersheds to storms within the humid region. The tracer studies for runoff

and streamflow had accelerated when they arose the questions where the rainwater goes? what flow paths it takes? and how long it stays in the catchment?

A much influential work was done by Pinder and Jones (1969) on the determination of the groundwater component of peak discharge from the total runoff chemistry. A chemical mass balance relation on the total, direct and groundwater runoff has used for this study. They have determined the solute concentration of the groundwater from the samples collected from baseflow and the chemical characteristics of the direct runoff from the collected samples from different direct runoff locations. They have inferred from the study that the groundwater runoff constitutes 32 % to 42 % of the peak discharge for the analysis period in the three watersheds of Nova Scotia.

Rodhe (1981) presented a paper at the Nordic Hydrological Conference based on his study using Oxygen-18 isotope as a tracer for separating the stream discharge into flows from groundwater and snowmelt runoff. For the study, he selected two catchments of areas 6.6 km^2 and 4.0 km^2 in Southern Sweden during the 1979 snowmelt. The variation of $\delta^{18}O$ in the precipitation made the $\delta^{18}O$ of snowmelt runoff different from that of groundwater. This made the hydrograph separation possible. The study showed that the groundwater flow contribution is the major part of the streamflow (70 % to 90 %) and the snowmelt and precipitation contributes to 10 % to 15 % of the catchment area.

Lehman and Ahuja (1985) made a study on interflow of water and tracer chemical on sloping field plots with exposed seepage faces with potassium bromide as the tracer. They conducted the experiment on four experimental plots, each 1.8 m wide and 8.0 m long on 6-8 % slope. The experimental field plots were isolated from each other and the surrounding area by sheet metal plates extending from 0.15 m above to 0.9 m below the surface. An open soil face of 0.7 m deep formed the lower end of each plot in a runoff monitoring pit. The plots were used to monitor tracer and water flows when simulated rainfall was applied. From the observations they concluded that transport of chemical in interflow and runoff might be substantially reduced with appropriate management of relatively small soil surface

and volume. They have also observed that water and tracer came primarily from an average distance of only 1.3 m upslope from outlet faces which are in close agreement with theoretical values for steady flow conditions.

The study of Oxygen-18 fractioning during the event of snowmelt in Vastrabacken forested headwater catchment, Northern Sweden by Laudon *et al.* (2002) for defining the origin areas of old and new water has greatly developed the understanding of water, solute, and contaminant discharge to streams. Because of the fractionation during snowmelt, there occurs a variation in snowmelt isotopic composition. This affects the accuracy in hydrograph separation of the spring flood events. So they presented an accurate method which accounts the temporal change in the snowmelt isotopic signal and the storage of meltwater in the watershed. They have found that only 17 % to 28 % meltwater left the catchment during the spring flood events. Thus a major portion of the meltwater is stored in the catchment.

Tirumalesh *et al.* (2007) carried out hydro chemical, environmental isotope and injected radiotracer investigations for finding the possible source of groundwater pollutants and their flow path at the site of Indian Rare Earths Ltd., Cochin, Kerala, India. Samples of water were collected from dug-out wells, piezometers and Periyar river in and around the site and analysed for physical parameters, chemistry and isotopes. Based on their investigation it was concluded that the groundwater is getting contaminated from the southern part of the Indian Rare Earths campus. The possible source area for the contamination could be the Fertilizer and Chemical of Travancore industry which is situated at the southern part of Indian Rare Earths campus.

Leibundgut and Seibert (2011) have done a detailed review on the applications of hydrological tracers and its methodology. They reviewed all the types of hydrological tracers and mentioned their importance. They have also mentioned that the physiochemical parameters can be treated as a relevant hydrological tracer.

After a flood event in the Lauchert river, Germany, it was assumed that the floodwater would have infiltrated into the karst system and transported towards the springs in the Danube valley. A dye tracer experiment was done by Knoll and Scheytt (2017) between the Lauchert river and Danube valley for getting insight into the subsurface flow directions and to study the preferential connections between the surface catchment of Lauchert and the Danube valley springs. They used sodium-fluorescein as a tracer and applied into the unsaturated zone. The tracer breakthrough curves at the springs showed that three of the five springs in the Danube valley were fed by the groundwater generating from the Lauchert surface catchment. The results also helped to explain the significant difference between flood damage in the central and lower courses of Lauchert river.

2.3.3 Geophysical Methods

The three-dimensional form of soil structure could be recorded conveniently using axial X-ray computed tomography scanning. Pierret *et al.* (2002) used this unique technique for tracing the interconnected macropores in the CT scans of a set of unobstructed soil samples brought from a Swiss pre-alpine meadow where *Aporrectodea nocturna*, a new earthworm species, was unintentionally introduced. After that three-dimensional mathematical morphological filters were applied for quantifying the reconstructed structure of the interconnected macropores. The results from their study implied that the introduction of the colony new species of earthworms induced almost no change to the soil structure. They observed no change in total length and mean diameter of macropores. However, there was an increase in the average lengths of individual macropores and found to be more vertical and farther apart at some depths were the new earthworm species have colonized.

Holden (2004) studied the hydrological connectivity of soil pipes by ground-penetrating radar (GPR) tracer detection. He used this technique to identify and map the soil pipes in blanket peat catchments in Pennine hills, England. He tested the ability of GPR in identifying hydrological connectivity of soil pipes using a tracer solution (Sodium Chloride) because GPR alone cannot determine the hydrological

connectivity between two cavities. The tracer solution was injected into the cavities which were already detected by GPR. Downslope to the injection points, GPR was placed and located on the ground directly above identified soil pipes. Significant variation in reflectance was evident from the resultant radargrams from some of the cavities and no variation from the others. The samples of pipe waters were collected for checking the GPR results. When the background levels were approximately doubled, the changes in electrical conductivity of the pipe water could be spotted by GPR without any processing of the data. Thus it was possible to promptly ascertain the hydrological connectivity of soil pipes within the dense pipe systems across the hillslopes devoid of any surface disruption. The remote measurement of travel times through the pipe networks was also found possible.

Luo *et al.* (2008) investigated a 10 cm in diameter and 30 cm in length unbroken soil column taken from the Pennsylvania State University's R.E. Larson Agricultural Research Centre at Rock Springs in Centre County, Pennsylvania, using industrial X-ray computed tomography having a resolution of 105.5×105.5×125.25 μm for the quantification study of soil structure and preferential flow through intact soil structure. Computed tomography was used in their investigation because it gives non-destructive a method of observing soil structure as well as examining solute breakthrough in real-time. The soil column was scanned for getting the overall soil structure. The experimental procedure included injecting 60 g l^{-1} KI solution at 6.6 ml min^{-1} for about 23 h. Then they scanned two critical positions in the column and taken digital photographs to monitor the solute transport in real-time. For obtaining the overall solute mas distribution, at the end of the experiment, they scanned the whole column again. They observed morphologically different macropores such as earthworm burrows, root channels, and interconnected macropores and their different roles in solute transport which was found to be varying in different soil profile or horizon. Because of entrapped air which covered 9.8, 11.5, and 18.5 % of the macropore volume in the 0 to 12 cm, 12 to 23 cm and below 23 cm depth soil column respectively, only the biogenetic macropores in the subsurface were active in the solute transport.

Repeated electromagnetic induction (EMI) surveys were carried out by Zhu *et al.* (2010) for developing an improved soil map for a 19.5 ha agricultural landscape at the Kepler Farm of the Pennsylvania State University within an elevation range of 373 to 396 m. The widely used soil apparent electrical conductivity (EC_a) which is measured by EMI was used to understand spatial variability of the soil. Different meters *i.e.* EM38, EM31 and dualem-2 were used with different dipole orientations (horizontal and vertical) and different geometrics and compared. For generating an EC_a map for the study area, readings from each EMI survey were interpolated using ordinary kriging in ArcGIS 9.1. The resulted soil map had a higher accuracy of 87.1 % compared to the second-order soil map (47.1 %) of the area developed by the USDA-NRCS, with nearly 70 % of the soil cores out of the collected 147 soil cores matched with the generated map.

In order to shed light on the process of lateral preferential flow and its dynamics in a hillslope of a 7.9 ha forested catchment in central Pennsylvania, USA, Guo *et al.* (2014) conducted a study with the application of time-lapse ground-penetrating radar (GPR) along with an artificial infiltration. They developed a new protocol to recreate lateral preferential flow networks with a resolution of 1 cm based on their refined GPR data post processing algorithms and improved field experimental format. Concurrent soil water observation and field soil examination confirmed the lateral preferential flow locations mapped by time-lapse GPR surveys. In their study, they observed two types of lateral preferential flow networks, the network at the soil permeability divergences and that formed with the series of connected preferential flow paths. It was also evident that the formation, as well as the distribution of lateral preferential flow networks, are subjective to the antecedent soil water circumstance. They concluded their study inferring that sensibly designed time-lapse GPR surveys together with enhanced post processing of the data bid a practical and conservative way of mapping lateral preferential flow networks in the field.

MATERIALS AND METHODS

CHAPTER III

MATERIALS AND METHODS

This chapter describes the study area and the details of the experimental setup for the collection of data and its analysis.

3.1 DESCRIPTION OF THE STUDY AREA

The experiments for the study were conducted in the KCAET campus, Kerala, India. The study area comprises of lateritic terrain having sandy loam type of soil and a gentle slope. It is situated at 10^{o} 51'18" N latitude and 75^{o} 59'11" E longitude at an altitude of 10 m above mean sea level. The average annual rainfall varies from 2500 to 2900 mm. The average maximum temperature of study area is 31 ºC and average minimum temperature is 26 ºC. The contour maps for the two experimental sites used for the study were developed using total station surveying.

3.2 EXPERIMENTAL SETUP

The whole study has been conducted on two sites with three experimental setups and the details of the same are given under.

3.2.1 Experimental setup 1

The experimental setup 1 was made at the first site having a general slope of 5 %. A through-flow trench of length 6 m, width 0.6 m and depth 1.8 m has been excavated on the first site at the downstream end across the general slope. For simulating the rainfall, a butterfly sprinkler was fixed at the centre of the plot, 8 m upslope to the through-flow trench. The plan view of the experimental setup and the section view of the throughflow trench is shown in figure 3.1.

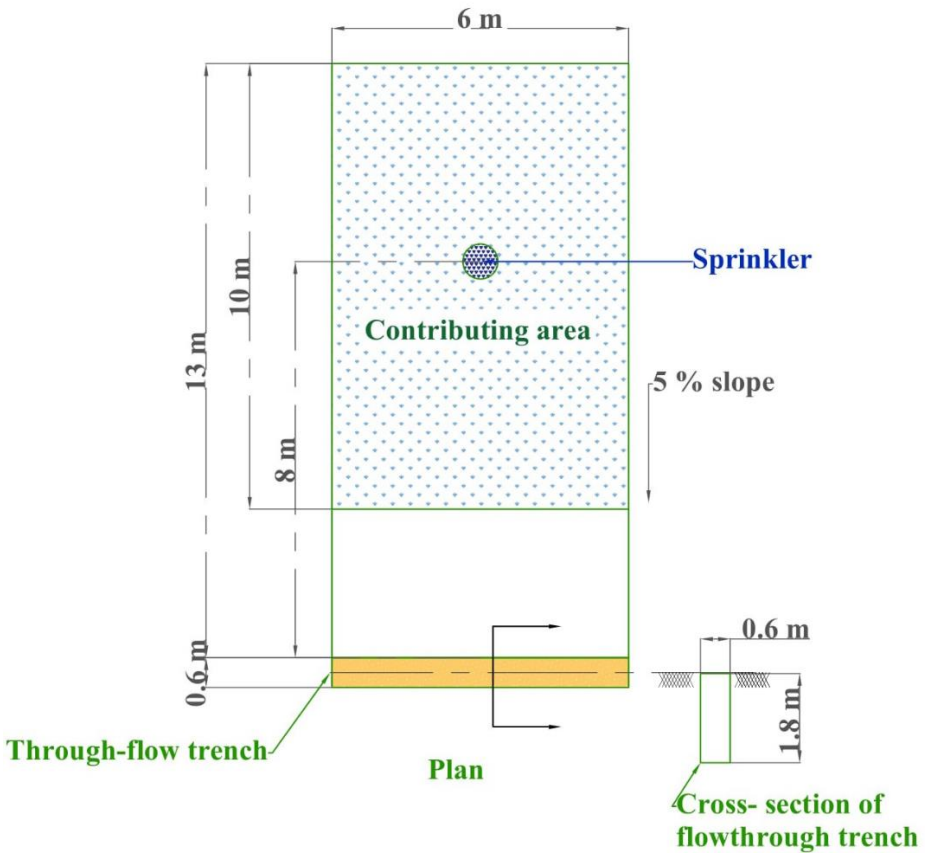

Figure 3.1 Schematic of experimental setup 1

The sprinkler was operated 12 hours a day, from 6 am to 6 pm, for three days in succession. The specifications of the sprinkler are given in table 3.1

Table 3.1 Specifications of the butterfly sprinkler for rainfall simulation

Operating Pressure (kg cm^{-2})	**Discharge (l h^{-1})**	**Radius of Coverage (m)**
1	660	5.00
1.5	780	5.20
2	900	5.35

The sprinkler is operated at a pressure of 1 kg cm^{-2} using a centrifugal pump of 1 hp connected to a nearby farm pond. It gave a spray diameter of 10 m and uniformity coefficient 90.87 % while operating at 1 kg pressure. Thus a contributing

area of 10×6 m is obtained for the through-flow trench. The moisture content on the trench face for the depths 0-40 cm, 40-80 cm and 80-120 cm were measured from 6 am to 6 pm at two-hour interval. The throughflow trench was covered using a polythene sheet to eliminate the entry of any direct water.

3.2.2 Experimental setup 2

The experimental setup 2 has made by excavating a through-flow trench of 3 m length, 0.6 m width and 1.6 m depth on the second plot across the general land slope, in order to intersect the subsurface flow coming from the upslope area. A small trench of length 2 m, width 0.3 m and 0.3 m depth was also constructed at 4 m upslope to the through flow trench to facilitate the supply of water. The diagrammatic representation of experimental setup 2 is shown in figure 3.2.

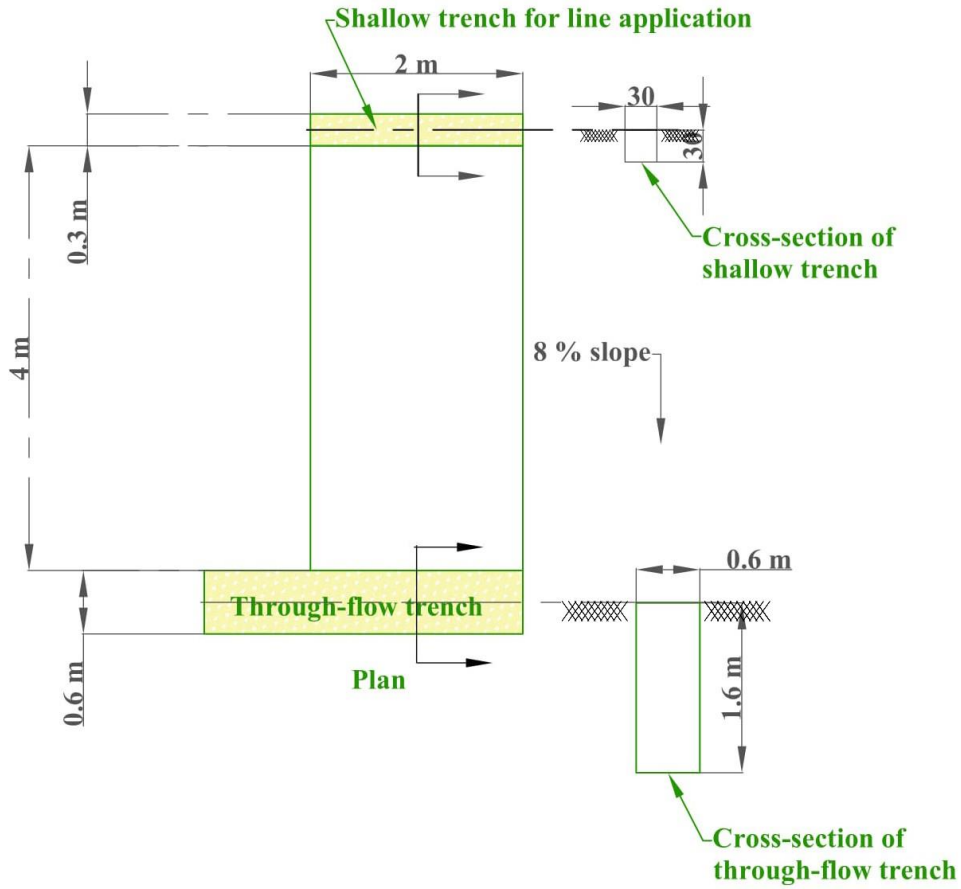

Figure 3.2 Schematic of experimental setup 2

In order to facilitate the generation of subsurface flow, the shallow trench was filled with water frequently for a consecutive 10 days' period. Water infiltrated from the trench is replenished regularly. Thus the infiltrated water is expected to flow towards the through-flow trench. The through-flow trench face was divided into three depths, *i.e.* 0 to 40 cm, 40 to 80 cm and 80 to 120 cm for determining the spatial variation in the subsurface stormflow throughout the trench profile by soil moisture measurement. For that the soil moisture at the trench face is observed after the line application of water into the shallow trench.

3.2.3 Experimental setup 3

The experimental setup 2 was used for the study in the pre monsoon season. In the monsoon season the plot used in experimental setup 2 was converted to experimental setup 3. A channel for diverting the surface runoff from the upslope areas was constructed to prevent the entry of surface runoff to the through-flow trench. The through flow trench as well as an area to 1 m upslope of the through-flow trench was covered using a tarpaulin sheet for restricting the fall of direct rainfall to the through-flow trench. The through-flow trench face was divided into three depths for determining the spatial variation in the subsurface stormflow throughout the trench face similar to that in experimental setup 2. The soil moisture monitoring was done at the trench face for these depths for a consecutive 15 days due to rainfall from 31-07-2019 to 14-08-2019. The diagrammatic representation for the experimental setup 3 is given in figure 3.3.

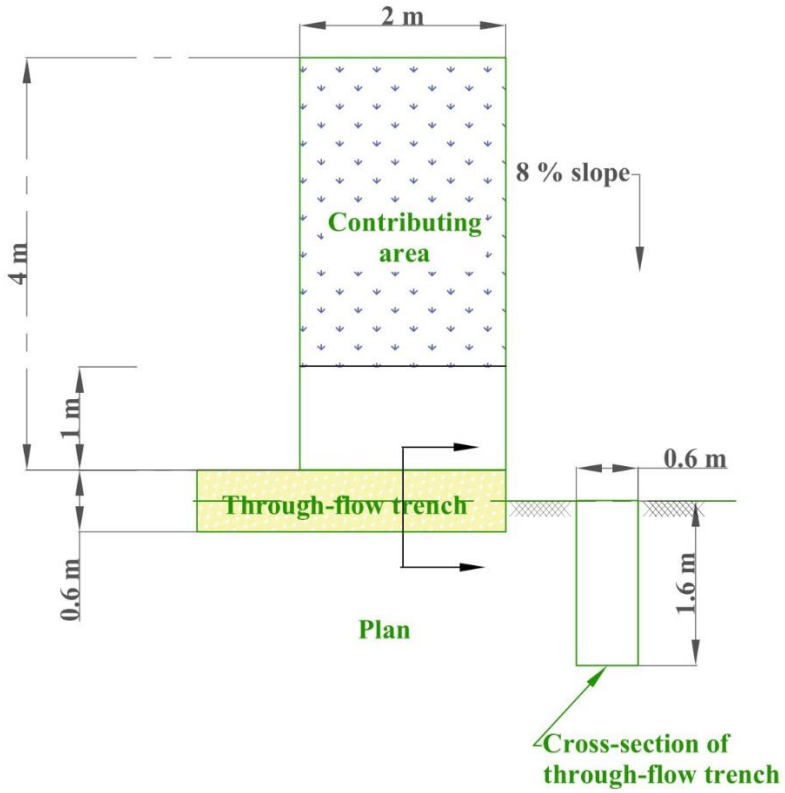

Figure 3.3 Schematic of experimental setup 3

3.3 DETERMINATION OF SOIL PHYSICAL PROPERTIES

The representative soil samples were collected from the profile depths 0-40 cm, 40-80 cm and 80-120 cm for the study plots for the determination of physical properties such as bulk density, specific gravity and particle size distribution. The methodologies used for the analysis of different soil samples are given in table 3.2.

Table 3.2 Soil physical properties and their method of determination

Physical Property	**Methodology**
Bulk density	Core cutter method
Specific gravity	Pycnometer method
Soil Texture	Sieve analysis
Moisture content	Oven drying and using TEROS 12 sensor

3.4 MEASUREMENT OF SOIL MOISTURE AND EC

The physio-chemical parameters such as the volumetric moisture content, electrical conductivity could be used as a hydrological tracer (Leibundgut and Seibert, 2011). The subsurface stormflow movement within the soil matrix will reflect on the change in the volumetric moisture content in the soil profile. So the analysis of volumetric moisture content within the specified depths in through-flow trench face is carried out to determine the spatial and temporal variation of the subsurface stormflow from the contributing area.

The soil moisture measurement for the experimental setup 1 and 2 has been carried out by measuring the soil moisture gravimetrically.

The measured gravimetric moisture content is converted into volumetric water content for quantification purpose using equation 3.1.

$$\theta = w \times \frac{\rho_d}{\rho_w} \tag{3.1}$$

Where *'θ', 'w', 'ρ_d'* and *'ρ_w'* are the volumetric water content, gravimetric moisture content soil dry density and density of water respectively.

The volumetric water content, EC and temperature of the soil for the experimental setup 3 are measured using three TEROS 12 capacitive sensors each fixed between the depths 0-40 cm, 40-80 cm and 80-120 cm on the through-flow trench face. The three sensors are plugged to a ZL6 data logger for data collection, data storage and data download. The ZL6 data logger could accommodate up to six different sensors in its six ports. The diagrams for the TEROS 12 sensor and the ZL6 data logger are shown in figure 3.4 and figure 3.5 respectively.

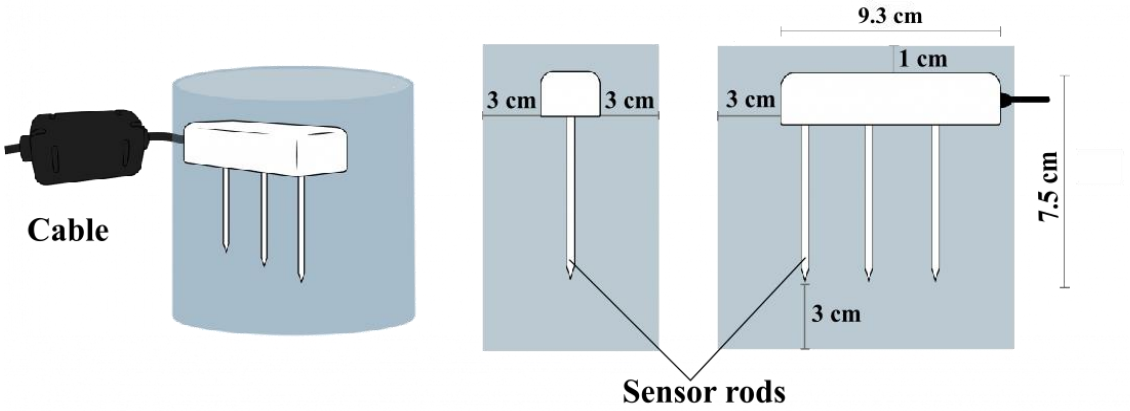

Figure 3.4 TEROS 12 capacitive sensor

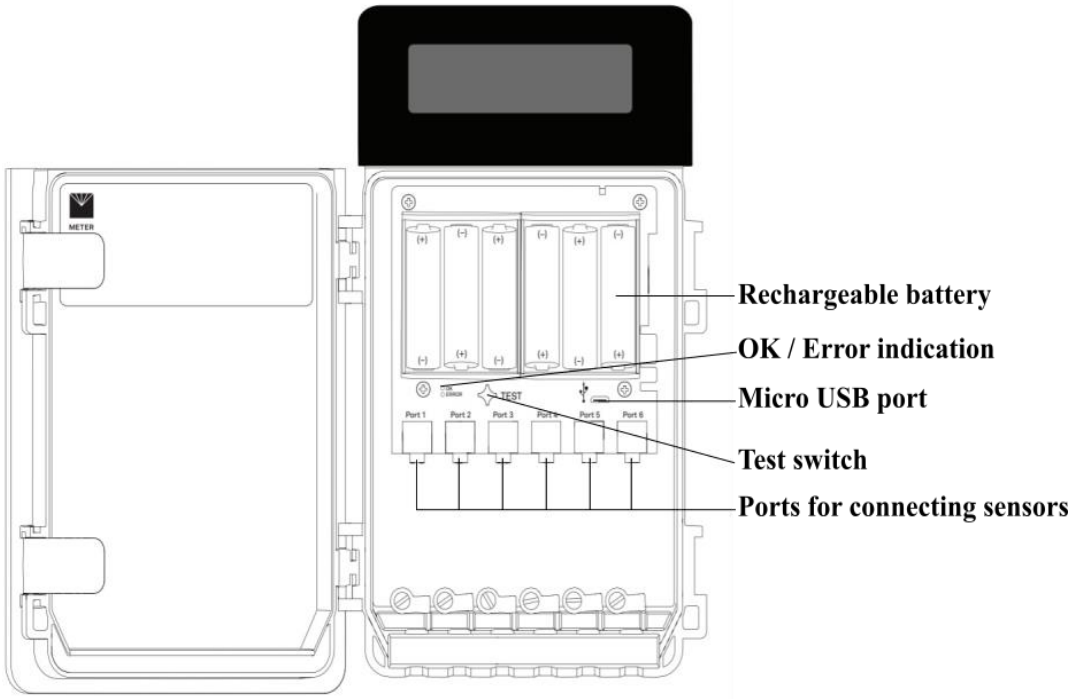

Figure 3.5 ZL6 data logger

Table 3.3 Specifications of TEROS 12 capacitive sensor

MEASUREMENT SPECIFICATIONS			
	Range	**Resolution**	**Accuracy**
Volumetric Water Content (m^3/m^3)	0.00–0.70	0.001	±0.03
Temperature (°C)	-40 to +60	0.1	±0.3
Electrical conductivity (dS m^{-1})	0-20	0.001	±(5% + 0.01)
Dielectric Measurement Frequency (MHz)		70	
COMMUNICATION SPECIFICATIONS			
Output	DDI serial or SDI-12 communication protocol		
Data logger compatibility	METER ZL6, EM60, and Em50 data loggers or any data acquisition system capable of 4.0- to 15-VDC power and serial or SDI-12 communication		
Operating temperature	-40 to +60°C		
PHYSICAL SPECIFICATIONS			
Dimensions (cm)	Length Width Height	9.4 2.4 7.5	
Prong Length	5.5 cm (2.17 in)		
Cable Length	5 m		
Connector Type	3.5-mm stereo plug connector		

Table 3.4 Specifications of ZL6 data logger

Sensor Input Ports	6 (supports METER analog, digital, or pulse sensors)
Sensor Port Type	3.5-mm stereo plug connector
Logging Interval	5 min to 12 h
Reporting Interval	Hourly with additional charges for more frequent reporting
Data Storage	8 MB (40,000 to 80,000+ records depending on configuration)
Memory Type	Nonvolatile flash, full data retention with loss of power
Global Position	Integrated 56-channel GPS/QZSS receiver
GPS Position Update	Daily (automatic) and on-demand (manual)
GPS Position Accuracy	±3 m, with good sky view
Timekeeping	Synchronize automatically and on-demand; GPS system, cellular, or software
Battery Capacity	6 AA NiMH or alkaline batteries
NiMH Battery Charging	Solar energy harvesting or USB
NiMH Battery Life	3+ years with an unobstructed view of the sun
Alkaline Battery Life	3–12 months depending on the configuration
Computer Communication	Standard USB cable, USB A to micro-B
3G Cellular Specifications	UMTS 3G 5-band Cellular Module with 2G fallback
3G Cellular Coverage	AT&T® and T-Mobile® in USA, 550+ global partner carriers. Cellular and data hosting service provided by METER.
4G Cellular Specifications	4G LTE-M and NB-IoT Cellular
Internet Downloads	SSL/TLS encrypted
Enclosure	Weather-, impact-, and UV-resistant polymer

The ZL6 logger stores the data to its storage as well as sends the data to the ZENTRA Cloud up to four times an hour, *i.e.*, once in every 15 minutes. This data could be downloaded using a personal computer either by connecting it with the ZL6 logger using a data cable with ZENTRA utility software installed on it or by connecting it online with ZENTRA Cloud. The same process is represented in figure 3.6.

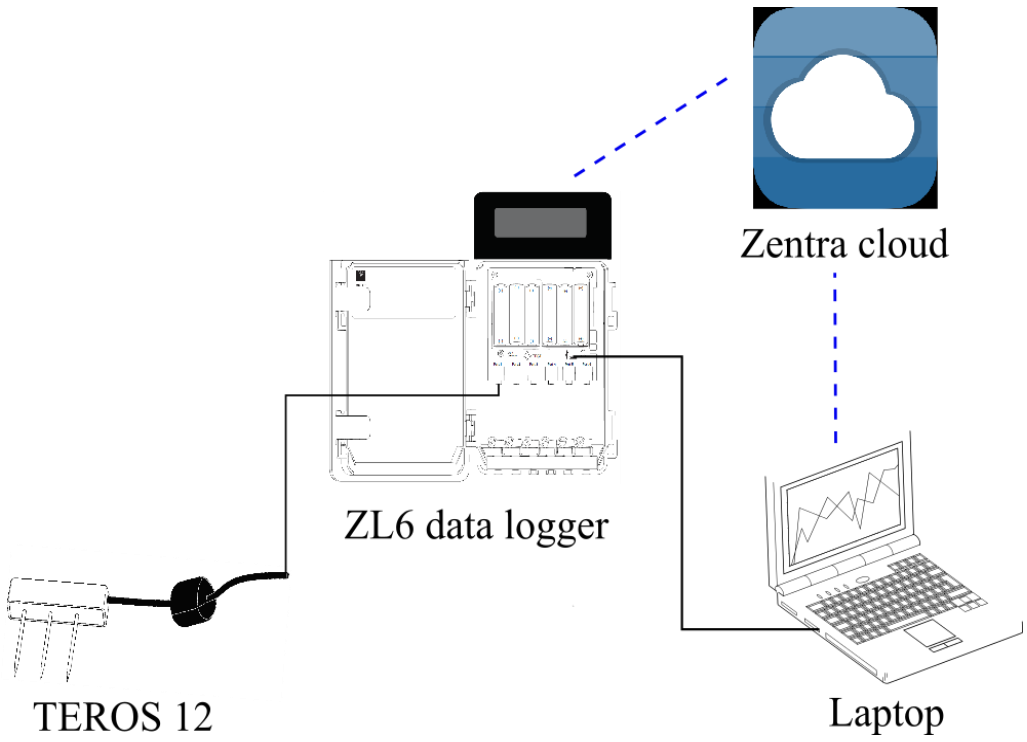

Figure 3.6 Diagrammatic representation of moisture measurement and data storage and download

3.5 MEASUREMENT OF RAINFALL

The daily rainfall data for the study area is obtained using the non-recording type Symons rain gauge installed in the meteorological observatory inside the KCAET campus. The 24 h rainfall data has been taken every day at 8.30 am.

3.6 TEROS 12 SENSOR CALIBRATION

3.6.1 Equipment needed

Table 3.5 Descriptions of the equipment needed for TEROS 12 calibration

Equipment Needed	Description
Shovel and soil bulk container	• For field soil collection and air drying soil. • 1 shovel, 1 container for each soil type.
Calibration container	• It should be large enough to pack the soil back to the field bulk density while maintaining enough soil depth to accommodate the full length of the sensor. • It should be relatively rigid and allows clear access to the soil surface.
Sensor and data acquisition system	• Three TEROS 12 sensors are calibrated for the three depths of the study area. • ZL6 data logger connected to ZENTRA utility is the data acquisition system
Weighing balance	• It is able to weigh upto 10 kg and is having a resolution of 0.2 g.
Soil drying containers	• It should be suitable for oven drying and has a sealable lid. • Each container should be weighed before adding soil to them.
Drying oven	• It should maintain a relatively stable temperature of 105 to 110℃.

3.6.2 Soil sample collection

Approximately four litres of soil samples for each of the three depths were collected from the study area. Soil samples were collected for determining the field bulk density of the soil for the three depths using core cutters.

3.6.3 Soil preparation

The collected sample was air dried by spreading it in a thin layer and the air is allowed to move over the soil and was kept for about 24 hr as shown in plate 3.1. After that, the large materials in the sample were removed by sieving the soil sample through 4.75 mm sieve and the large clods found were broken down because these objects will complicate the calibration process.

Plate 3.1 Soil sample kept for air drying in a thin layer

3.6.4 Calibration procedure

The chronological steps involved in the calibration procedure are as follows;

1. The soil is gently added to the calibration container layer by layer so as to maintain the measured field bulk density for each layer. The bulk density is attained by packing a known volume of soil into the known volume of the container. The packing of soil sample is shown in plate 3.2.

Plate 3.2 Soil sample is being packed in the calibration container

2. A small amount of the packed soil sample is taken in a soil drying container of known weight and measured the weight of drying container + soil sample. Then any void occurred in the packed soil was replaced. Then the sample kept for oven-drying in 105^{o}C for 24 h.
3. The entire calibration container with soil has been weighed.
4. The TEROS 12 sensor was inserted into the packed soil after preparing a flat spot to fit the sensor as shown in plate 3.3. Then the soil is packed over the exposed portion of the sensor by maintaining the bulk density and preventing the air gaps. It was made sure that there is 1 cm of soil over the top of the sensor

Plate 3.3 Insertion of the sensor into the packed soil

5. Raw data (uncalibrated data) were collected using the data acquisition system (ZL6 data logger and ZENTRA utility software).
6. The calibration soil was made wet by adding 10 % water to the soil sample on volume basis. Then the soil was thoroughly mixed the soil until the mixture became homogeneous.
7. The steps 3 to 6 were repeated until the soil became near to saturation. This procedure yields 4 to 6 calibration points. It was ensured that the bulk density of the soil is maintained throughout the calibration process by packing the same amount of soil to the same volume of the calibration container.
8. Then the sample kept for oven drying in step 2 after 24 h was weighed with the container.

3.6.5 Finding and using the calibration function

For finding the calibration function a scatter plot is made with sensor output on X-axis and the calculated volumetric water content on Y-axis. Then a mathematical model of the relationship is constructed using the curve-fitting function in the spreadsheet. Then for using the calibration function, it is added to ZENTRA Cloud online under the System Settings tab in the Calibration Settings. This is achieved by entering the coefficients with enough significant figures after activating Add Calibration button.

3.7 SUBSURFACE STORMFLOW QUANTIFICATION THEORY

The main theory behind the subsurface stormflow quantification in this study is the concept of volumetric water content. It could be defined as the volume of water present in the unit volume of a given sample or column of soil. So the movement of water inside the soil column will reflect on the volumetric water content within the soil column.

Consider an imaginary soil column of unit width having length 'L' and height/depth 'H' as shown in figure 3.7. Assume its dry density and volumetric moisture content to be 'ρ_d' and 'θ_i' respectively.

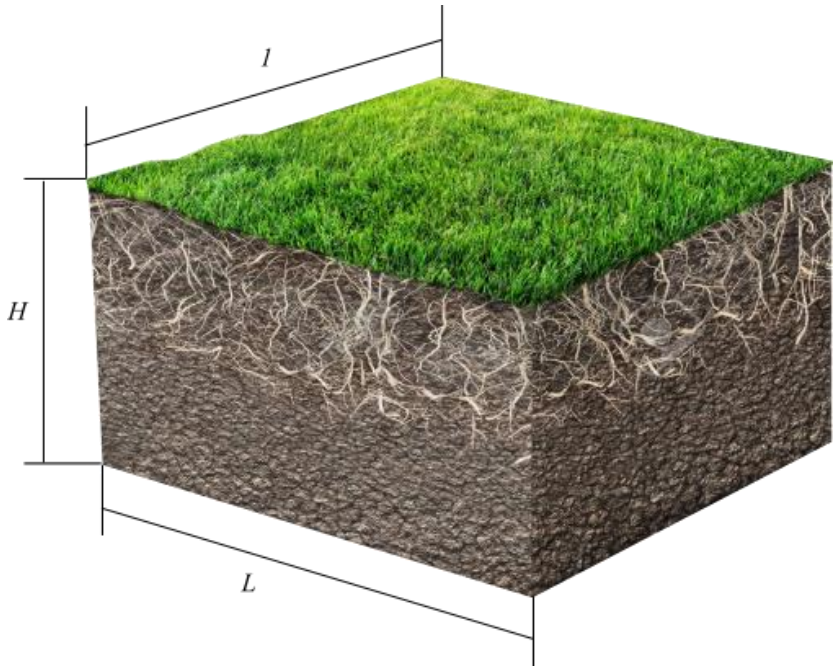

Figure 3.7 Imaginary soil column

At this instant the volume of water present in the soil column, 'V_i' can be obtained from equation 3.2.

$$V_i = L \times H \times 1 \times \theta_i \text{ cubic units} \quad (3.2)$$

After a period of time 't', if the volumetric water content increases to 'θ_f', then the volume of water present in the soil column then, 'V_f' is obtained from the equation 3.3.

$$V_f = L \times H \times 1 \times \theta_f \text{ cubic units} \quad (3.3)$$

Therefore, the volume of water entered into the soil column in time 't', 'V' can be determined using equation 3.4.

$$V = V_f - V_i \text{ cubic units}$$

$$V = L \times H \times (\theta_f - \theta_i) \text{ cubic units} \quad (3.4)$$

Let the discharge rate of subsurface stormflow through a cross-section area '*A*' be '*Q*', then the pore velocity can be determined using equation 3.5.

$$v = \frac{Q}{A \times porisity} \tag{3.5}$$

3.8 OBTAINING THE SOIL SUCTION DATA

The soil water characteristic curve is the relation between the soil water content and the suction for the soil. In order to obtain the soil moisture curve for the two plots at three different soil profile depths tensiometers were installed at the depths 0-40 cm, 40-80 cm and 80-120 cm on the trench face for each experimental plots. The variation in the moisture content is observed using TEROS 12 sensors and the corresponding soil suction is observed from the installed tensiometers. Later the soil water characteristic curves are made using the observations.

The total energy possessed by the fluid in an unsaturated soil matrix is the sum of gravitational force and the soil suction forces. The gravitation potential due to gravitation force will enhance the flow of fluid through the matrix while the suction potential due to soil suction force will resist the fluid flow. this is because of the attraction force between the soil particles and the fluid particles having opposite charges. The equation for the total head is given in equation 3.6.

$$h = \psi + z \tag{3.6}$$

Where h, ψ and z are the total head, the suction head and the gravity head respectively.

3.9 APPLICATION OF TRACER

In order to determine the subsurface stormflow velocities for different depths, tracer study is to be carried out. For that a small trench of length 50 cm, width 30 cm and depth 30 cm has been constructed on the second experimental plot. It is excavated 2 m upslope to the through-flow trench. Sodium chloride solution of 120 ppm is prepared and used as tracer. The solution is applied into the small trench frequently till the TEROS 12 sensors fixed at the trench face will detect the change

in EC which indicates the subsurface stormflow. The background EC value for the tracer solution is also determined.

RESULTS AND DISCUSSION

CHAPTER IV

RESULTS AND DISCUSSION

4.1 CONTOUR MAPS OF EXPERIMENTAL SITES

The contour maps for the experimental sites are obtained using total station surveying and are shown in figure 4.1 and figure 4.2.

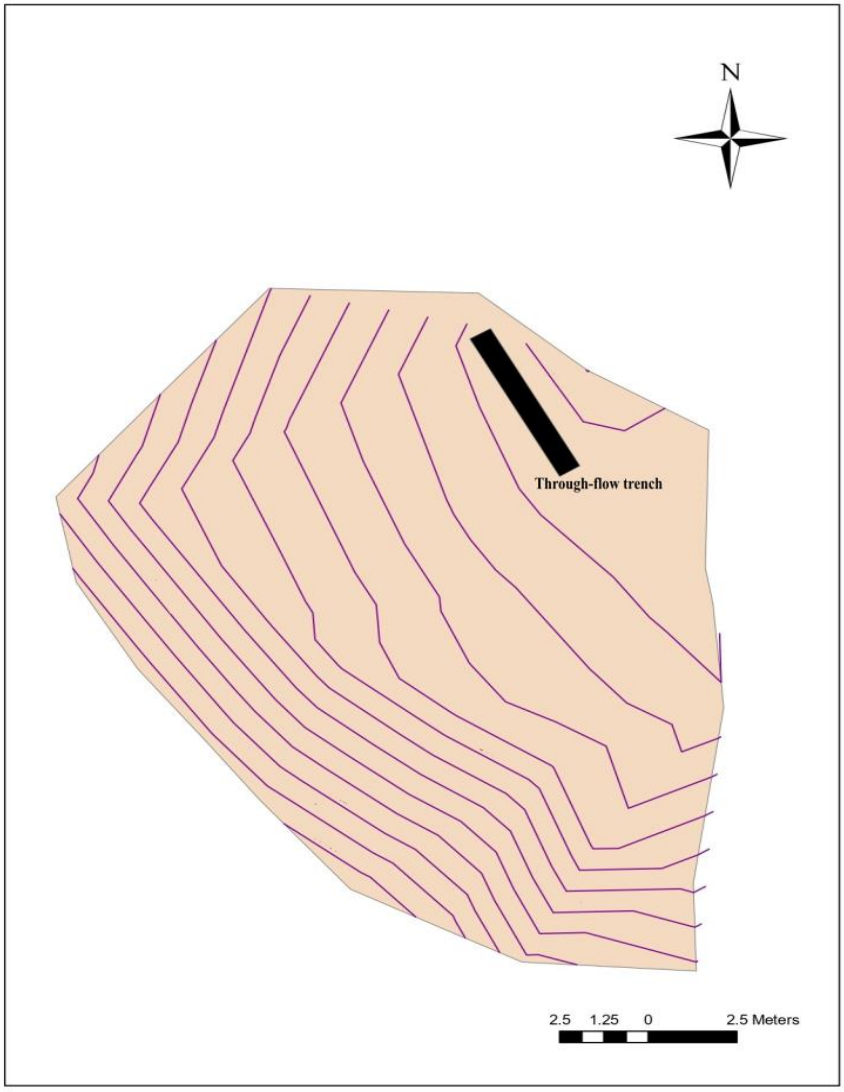

Figure 4.1 Slope map of first experimental site 1

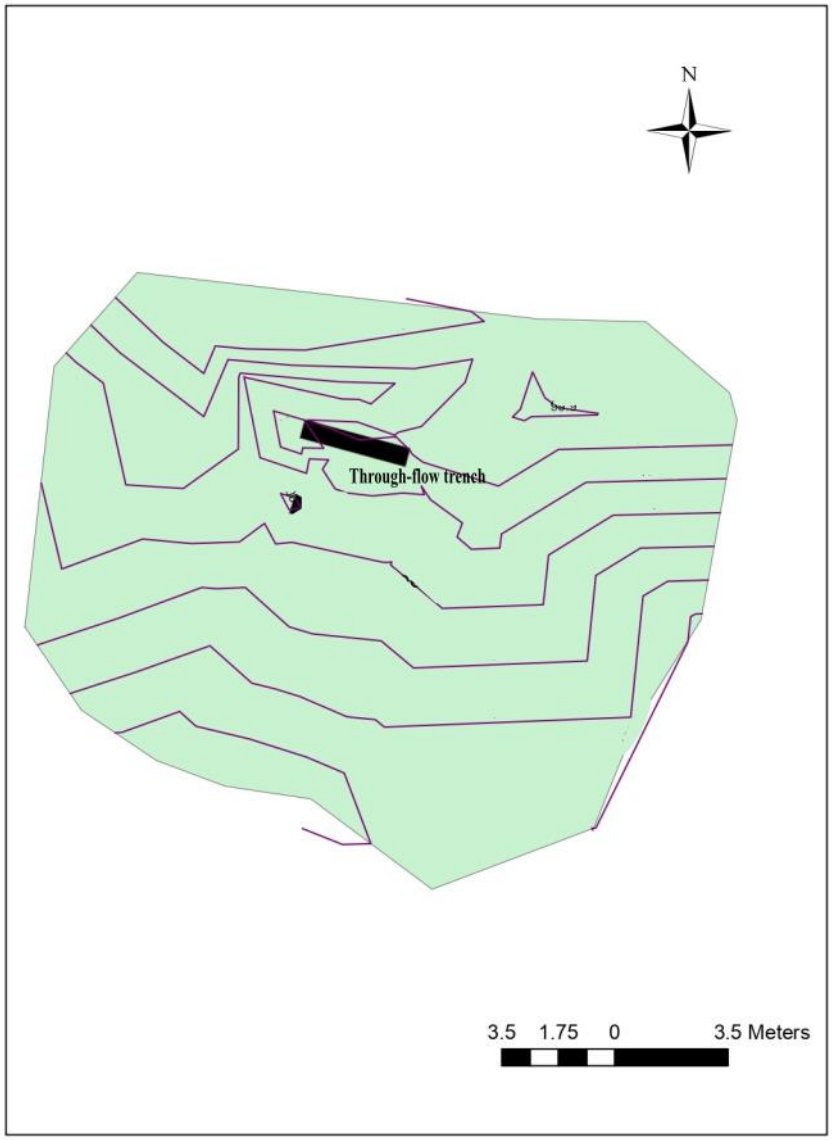

Figure 4.2 Slope map of second experimental site 2

4.2 SOIL PHYSICAL PROPERTIES

The soil physical properties for the study area have been determined using the standard procedure. Physical properties like dry density, specific gravity and texture for the three depths for the two experimental plots are presented in table 4.1.

Table 4.1 Soil physical properties for the experimental plots

	Physical Properties	Soil Depth		
		0-40 cm	40-80 cm	80-120 cm
First experimental plot	Dry Density (g cm^{-3})	1.16	1.56	1.58
	Specific Gravity	2.45	2.54	2.66
	Sand (%)	66.00	61.20	72.39
	Silt (%)	30.57	37.98	25.63
	Clay (%)	3.43	0.82	1.98
	Soil Texture	Sandy loam	Sandy loam	Loamy fine sand
	Porosity	0.53	0.39	0.41
	Void Ratio	1.13	0.64	0.70
Second experimental plot	Dry Density (g cm^{-3})	1.23	1.11	1.26
	Specific Gravity	2.42	2.49	2.54
	Sand (%)	76.46	75.03	71.36
	Silt (%)	18.40	19.70	22.47
	Clay (%)	5.14	5.27	6.17
	Soil Texture	Loamy fine sand	Sandy loam	Sandy loam
	Porosity	0.49	0.55	0.50
	Void Ratio	0.96	1.22	1

4.3 SOIL MOISTURE MEASUREMENT

4.3.1 Soil moisture monitoring for experimental setup 1

The soil moisture variation measured by gravimetry for the experimental setup 1 by simulating rainfall using sprinkler for three days is shown in figure 4.3, figure 4.4 and figure 4.5. Sprinkler operation was continuous from 6 am to 6 pm. The curves show the variations in the soil moisture movement.

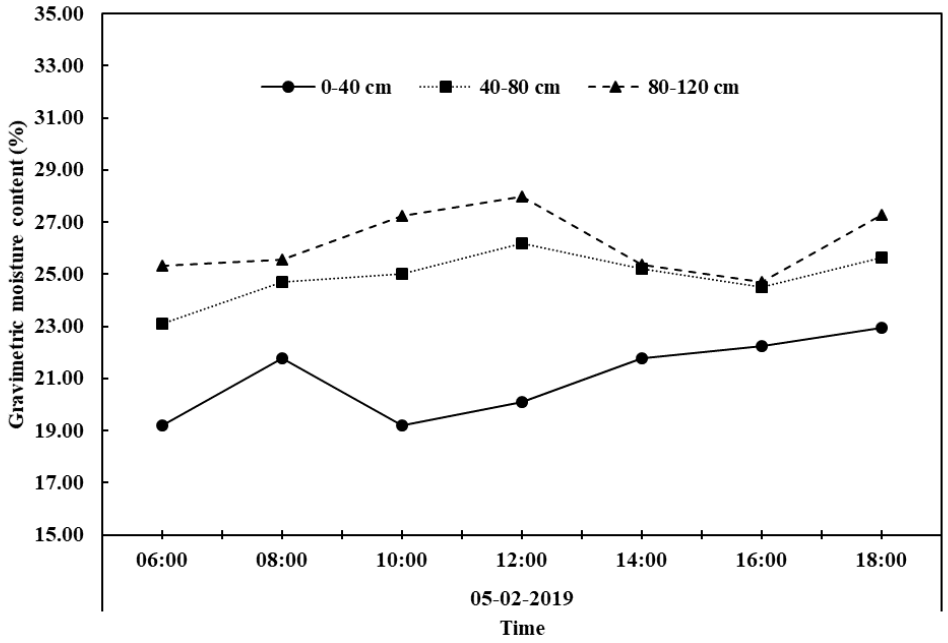

Figure 4.3 Gravimetric moisture values for experimental setup 1 on 05-02-2019

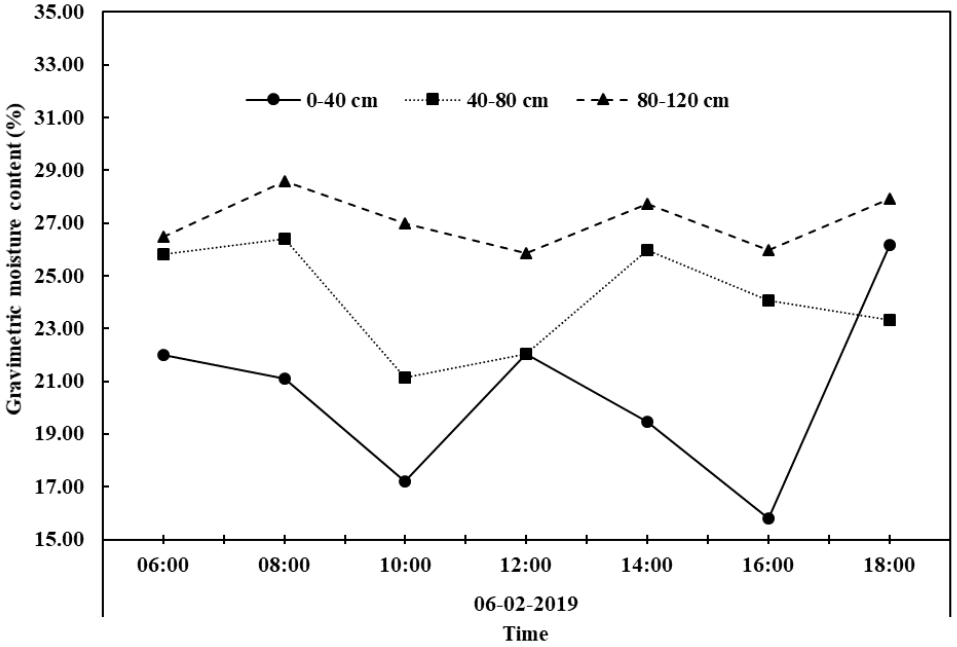

Figure 4.4 Gravimetric moisture values for experimental setup 1 on 06-02-2019

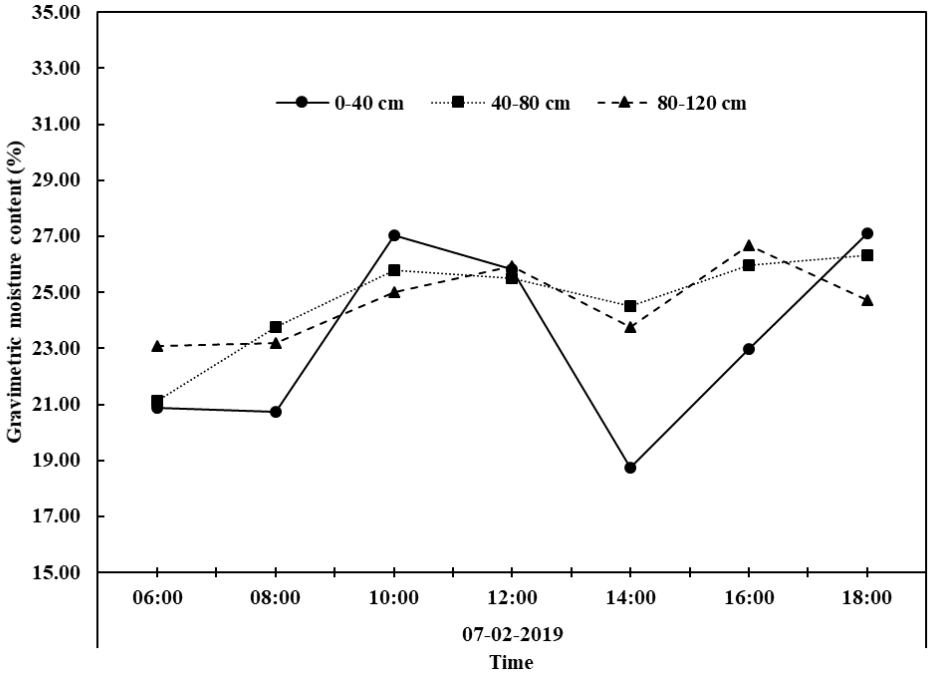

Figure 4.5 Gravimetric moisture values for experimental setup 1 on 07-02-2019

From the study conducted on experimental setup 1, both increase and decrease in the soil moisture values were observed. This may be due to the 12 h of water application (6 am to 6 pm) and the other 12 h of the off period (6 pm to 6 am) of rainfall simulation. The depth of water application of the sprinkler calculated from its specifications was 0.84 cm h^{-1}. Therefore, a total of 18144 litre of water has been artificially applied to the contributing area within a span of three days with 12 h day^{-1} of operation. By analysing the gravimetric soil moisture data for experimental setup1 monitored from 6 am to 6 pm for the three days of water application, it was found that out of the total rainfall simulated (18144 litre) for three days, a total of 2397.21 litre of water has been moved as subsurface stormflow which amounts to be 13.21 % of the total water application. It was also found that the subsurface stormflow discharge through the depths 0-40 cm, 40-80 cm and 80-120 cm were 190.76 l m^{-2} day^{-1}, 79.52 l m^{-2} day^{-1} and 62.68 l m^{-2} day^{-1} respectively. The subsurface flow through these depths as percentage of the total simulated rainfall were 7.57 %, 3.16 % and 2.49 % respectively.

4.3.1.1 Discharge versus time graph for experimental setup 1

The subsurface stormflow discharge per unit cross-sectional area versus time graph for the three days are potted and are shown in figure 4.6, figure 4.7 and figure 4.8.

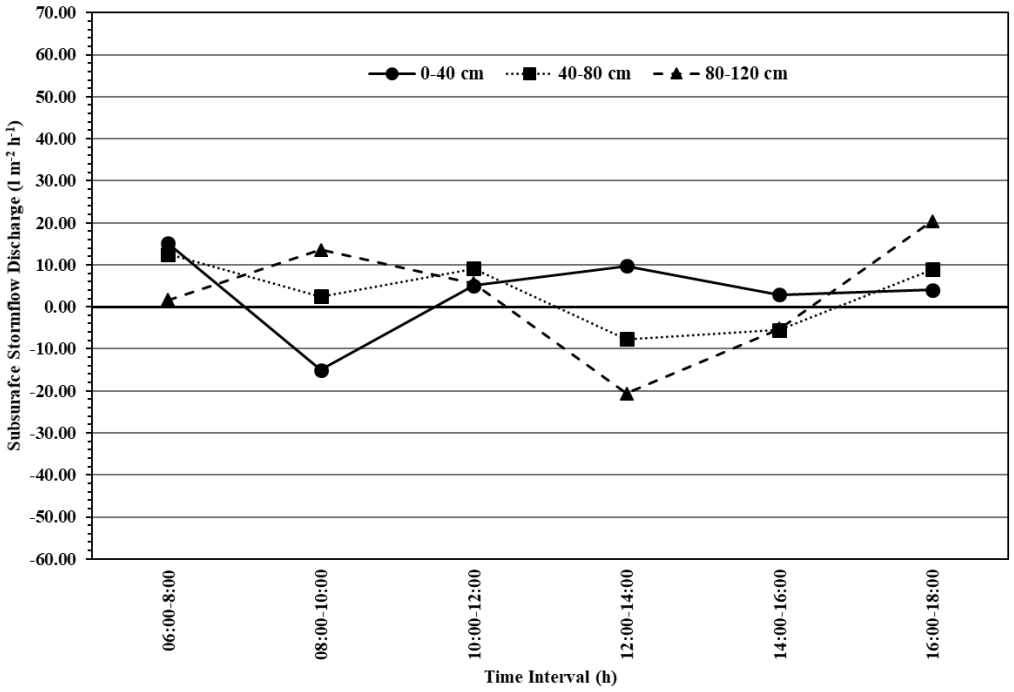

Figure 4.6 Subsurface stormflow discharge versus time graph for 05-02-2019 for experimental setup 1

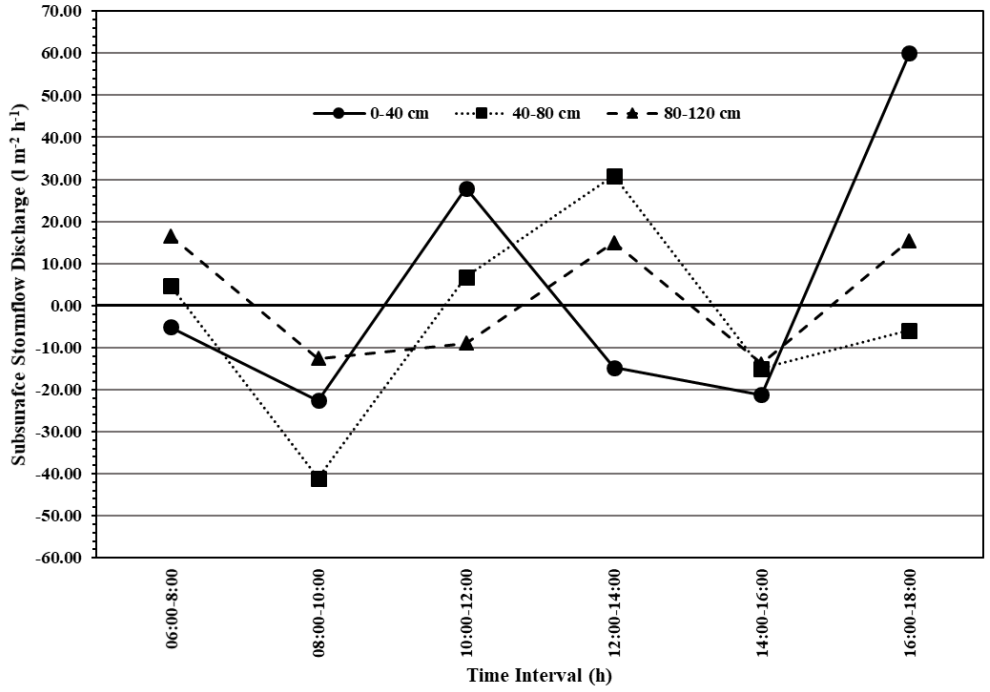

Figure 4.7 Subsurface stormflow discharge versus time graph for 06-02-2019 for experimental setup 1

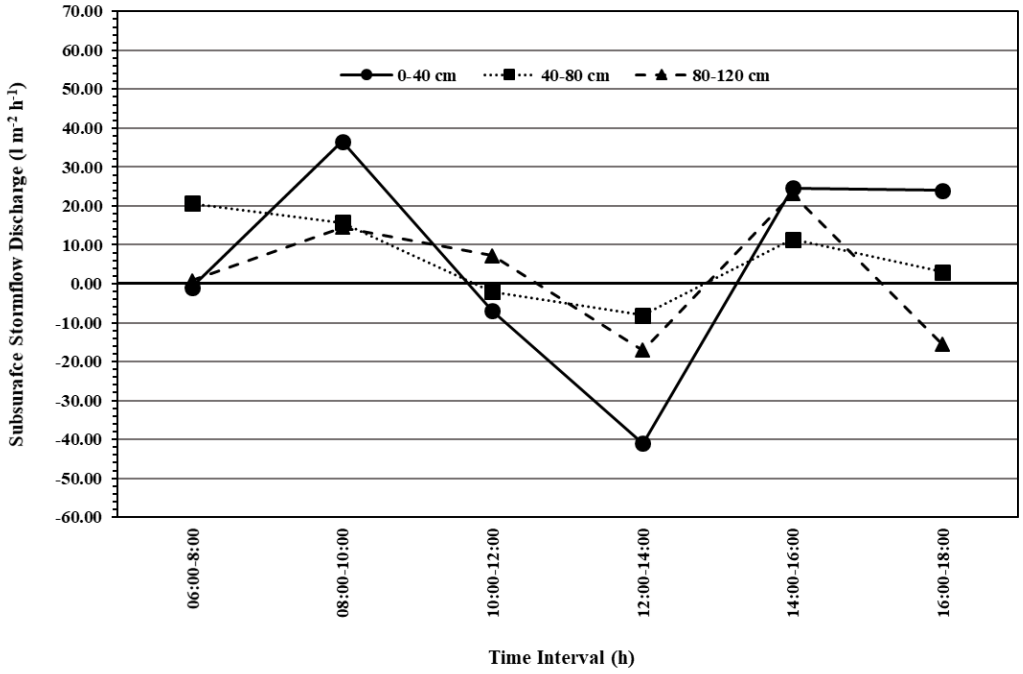

Figure 4.8 Subsurface stormflow discharge versus time graph for 07-02-2019 for experimental setup 1

In the graphs shown above, the positive discharge indicated the occurence of subsurface stormflow and the negative discharge indicated the retrieval of the same or the moisture declining phase. The negative values of discharge were due to the lag in the simulation of rain during 12 h off period. From the graph it is evident that both the phases starts in the top 40 cm layer which is having less bulk density compared to other two layers. Therefore it is evident that the moisture variation on the top 40 cm layer is maximum even though the layer has got minimum moisture content in most scenarios.

4.3.2 Soil moisture monitoring for experimental setup 2

Water was intermittently applied to the shallow trench which is 4 m away from the through-flow trench face for consecutive 10 days. Water is fed to the shallow trench intermittently at adequate intervals so that there will be water always in the pit. The soil moisture movements were observed for 10 days by taking the soil moisture content for the three depths gravimetrically. It is represented in figure 4.9.

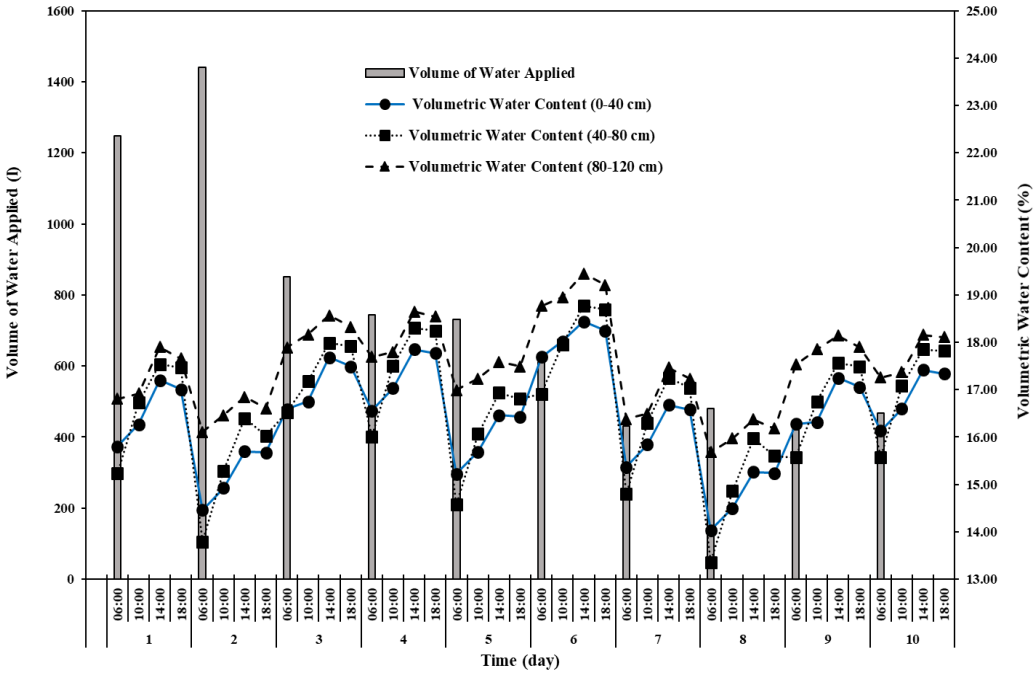

Figure 4.9 Soil moisture data for experimental setup 2

Line application of water into the shallow trench situated 4 m upslope to the through-flow trench for the experimental setup 2 resulted in variation of moisture content on the trench face. The decrease in the values of volumetric water content on the trench face was due to the off period of application of water from 6 pm to next day 6 am. A total of 7428 l water has been applied and out of that 340.64 l of water has transmitted as the subsurface stormflow. Therefore, 4.58 % of the applied water has been flowed as subsurface stormflow. The first, second and third 40 cm depths of the soil transmitted 27.74 %, 53.43 % and 18.84 % of the total subsurface stormflow. In terms of total applied water, 1.54 %, 1.61 % and 1.52 % got transformed into subsurface stormflow for the three depths respectively. The quantity of subsurface stormflow discharges through 0-40 cm, 40-80 cm and 80-120 cm depths were found to be equal to 11.80 l m^{-2} day^{-1}, 22.80 l m^{-2} day^{-1} and 8.00 l m^{-2} day^{-1} respectively.

4.3.2.1 Discharge versus time graph for experimental setup 2

The subsurface stormflow discharge per unit cross-sectional area versus time graph for the first five days of experiment is given in figure 4.10. The figure 4.11 represents the same for the last five days of the experiment.

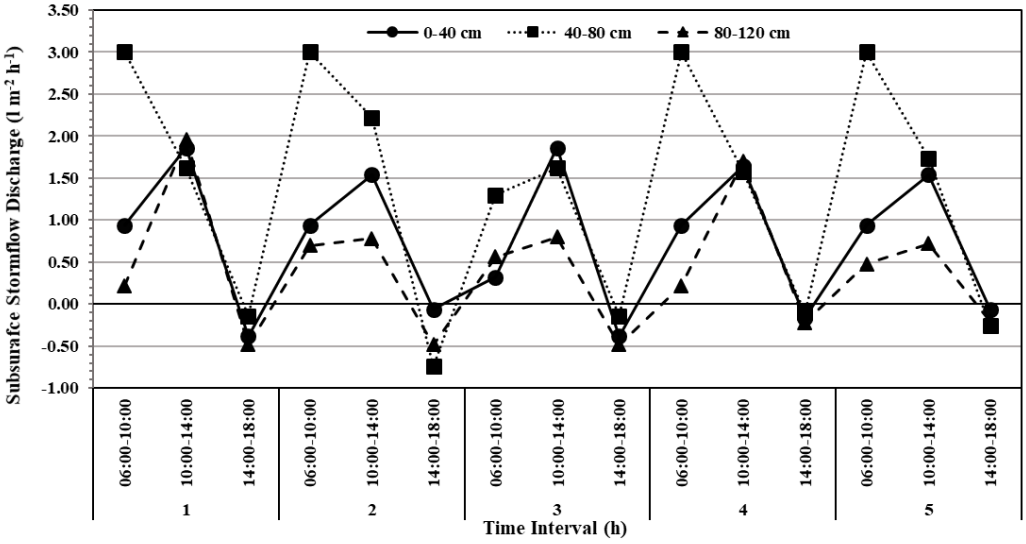

Figure 4.10 Subsurface stormflow discharge versus time graph for the first five days of experimental setup 2

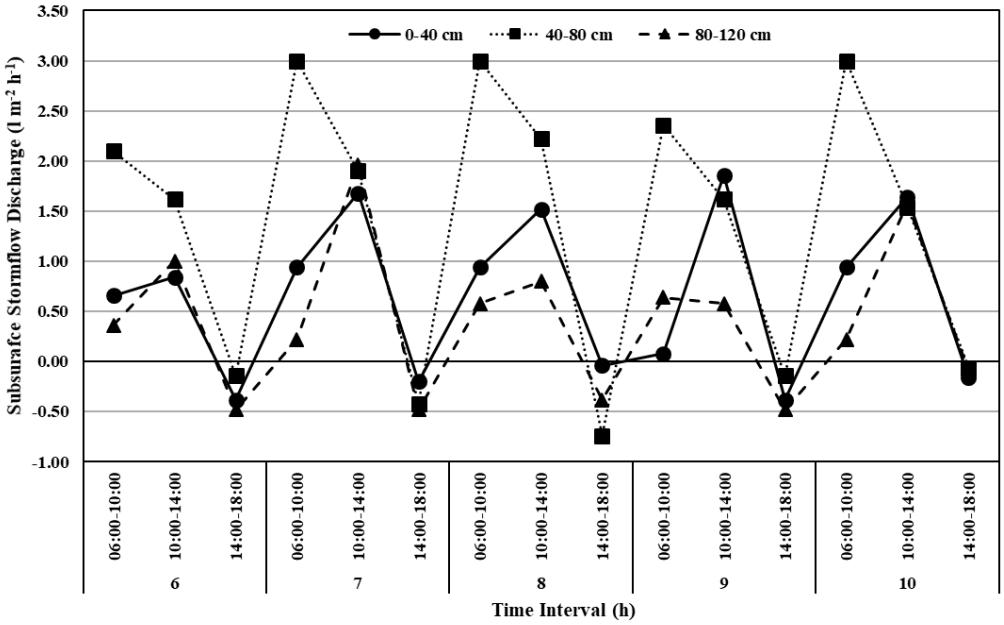

Figure 4.11 Subsurface stormflow discharge versus time graph for last five days of experimental setup 2

From the subsurface stormflow discharge versus time graphs for the experimental setup 2, it can be seen that the subsurface stormflow discharge is maximum for the 40-80 cm soil layer compared to the other two soil layers. Despite having low moisture content for 40-80 cm soil layer, which is having the minimum bulk density among the three layers, exhibits higher variations in the soil moisture data.

4.3.3 Soil moisture sensor calibration (TEROS 12)

All the three TEROS 12 sensors used in the study were calibrated for the three different depths of the experimental plot 2. The calibration curves, functions and the corresponding R^2 values of each sensor for their respective depths are given in figure 4.12, figure 4.13 and figure 4.14.

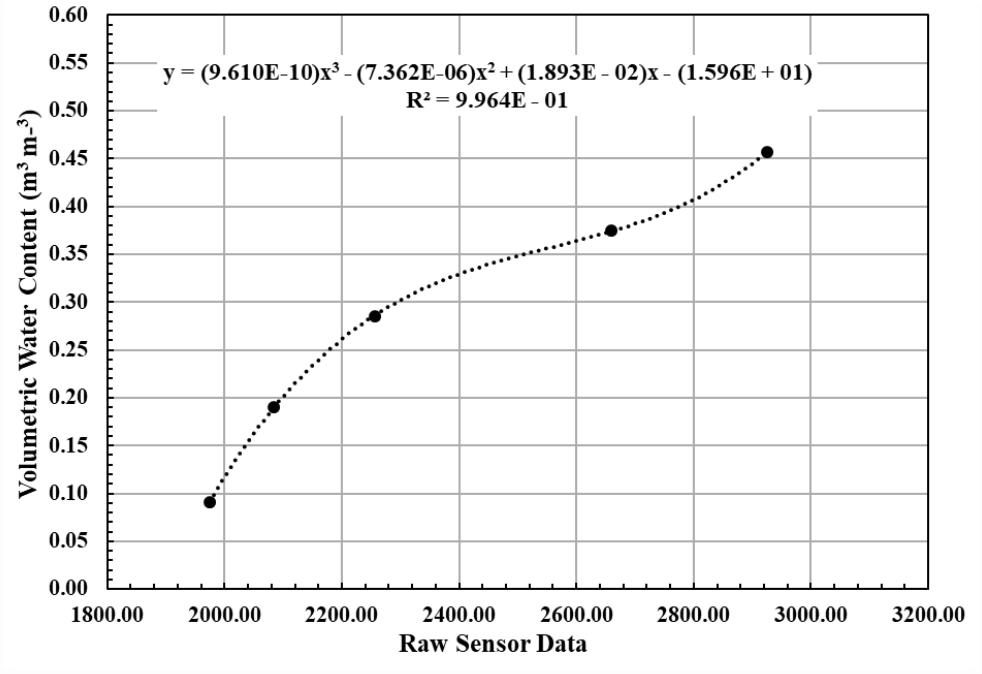

Figure 4.12 Calibration curve for sensor 1 (for 0-40 cm soil layer)

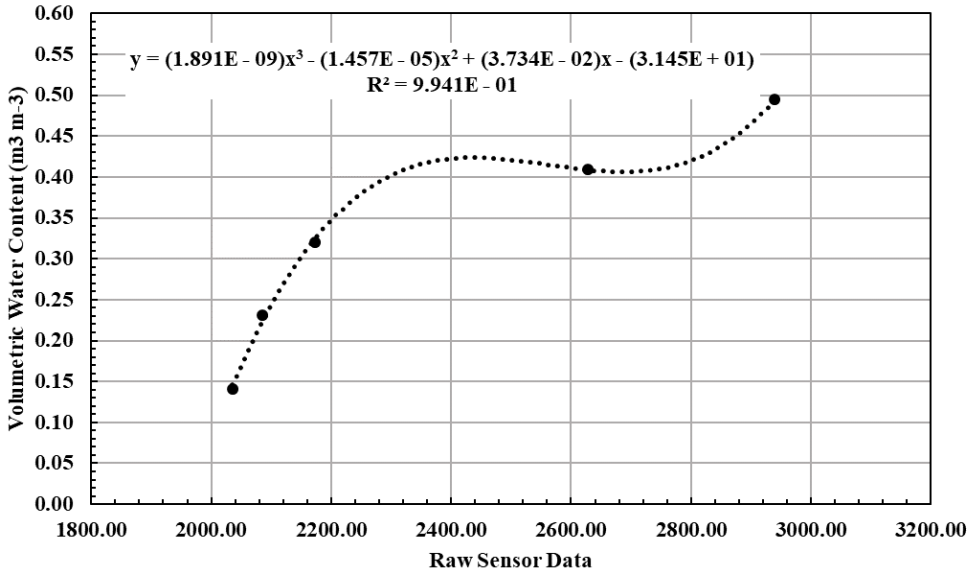

Figure 4.13 Calibration curve for sensor 2 (for 40-80 cm soil layer)

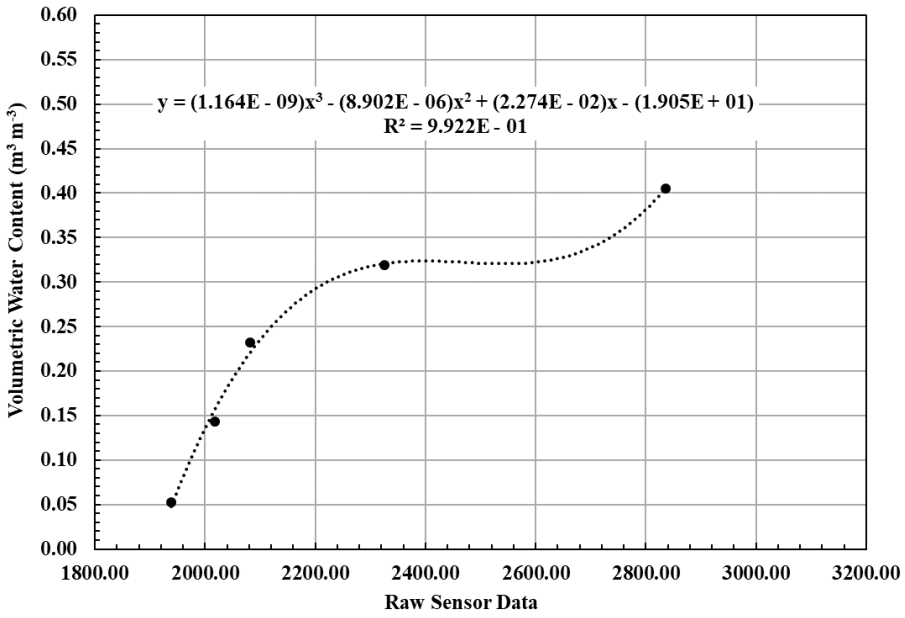

Figure 4.14 Calibration curve for sensor 3 (for 80-120 cm soil layer)

Table 4.2 Calibration functions for the sensors

Sensor	Calibration Function	R^2 Value (%)
1	$y = (9.610E - 10)x^3 - (7.362E - 06)x^2 + (1.893E - 02)x - (1.596E + 01)$	98.64
2	$y = (1.891E - 09)x^3 - (1.457E - 05)x^2 + (3.734E - 02)x - (3.145E + 01)$	98.42
3	$y = (1.164E - 09)x^3 - (8.902E - 06)x^2 + (2.274E - 02)x - (1.905E + 01)$	98.22

Here, for all the calibration the R^2 values are greater than 98 % which represents an excellent goodness of fit.

4.3.4 Soil moisture monitoring for experimental setup 3

The results of soil moisture monitoring by soil moisture sensors and data logger is presented here. Three TEROS 12 sensors, after calibration, were fixed on the trench face at three depths (0-40 cm, 40-80 cm and 80-120 cm) for taking hourly measure of volumetric water content for the corresponding depths. The sensors were connected to the ZL6 data logger as shown in plate 4.1. The soil moisture movement was measured under natural rainfall conditions.

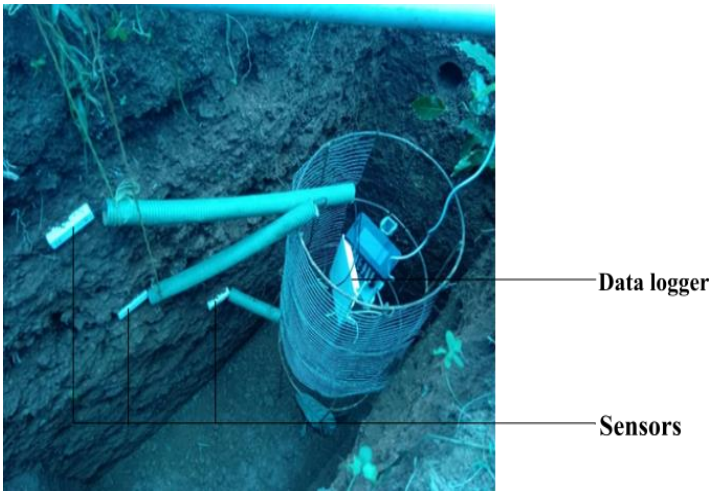

Plate 4.1 Arrangement of sensors and data logger on the trench face

Soil moisture data of trench face was taken in the monsoon season from 31 July 2019 to 14 August 2019. Up to 1 m from the trench face towards the upslope was covered by tarpaulin so as to eliminate direct rainfall on that area. This ensures any moisture increase on the trench face is only due to subsurface stormflow through the soil matrix. The 24-h rainfall data for these days are given in table 4.3.

Table 4.3 Rainfall data from 31 July 2019 to 14 August 2019

Date	Rainfall (mm)
31-07-2019	2.00
01-08-2019	5.60
02-08-2019	6.80
03-08-2019	6.40
04-08-2019	5.80
05-08-2019	8.20
06-08-2019	35.60
07-08-2019	2.00
08-08-2019	19.60
09-08-2019	107.40
10-08-2019	41.40
11-08-2019	13.60
12-08-2019	4.40
13-08-2019	20.00
14-08-2019	19.20

The soil moisture movement for the days on which the trench face exhibited significant variations in the moisture data within the period of the experiment are given from figure 4.15 to figure 4.21.

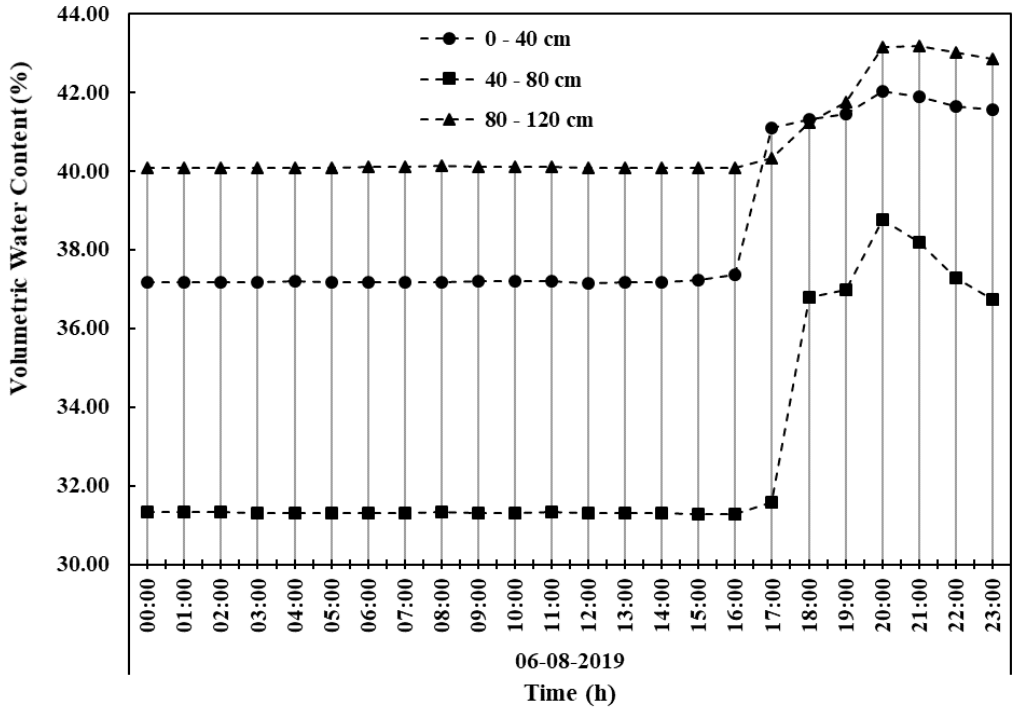

Figure 4.15 Soil moisture data of trench face for 06-08-2019

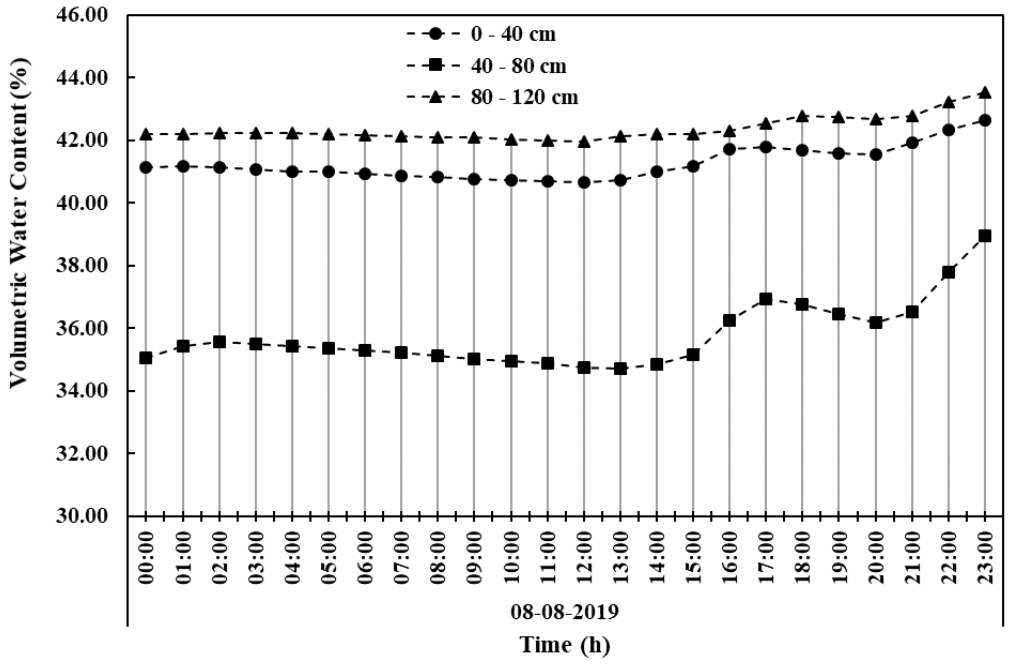

Figure 4.16 Soil moisture data of trench face for 08-08-2019

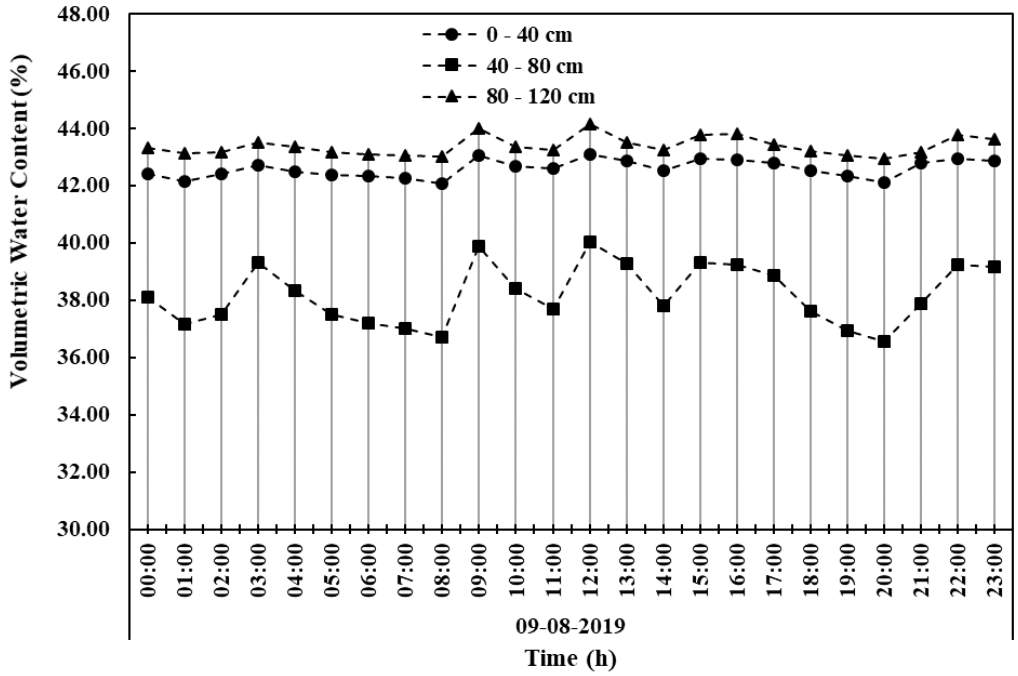

Figure 4.17 Soil moisture data of trench face for 09-08-2019

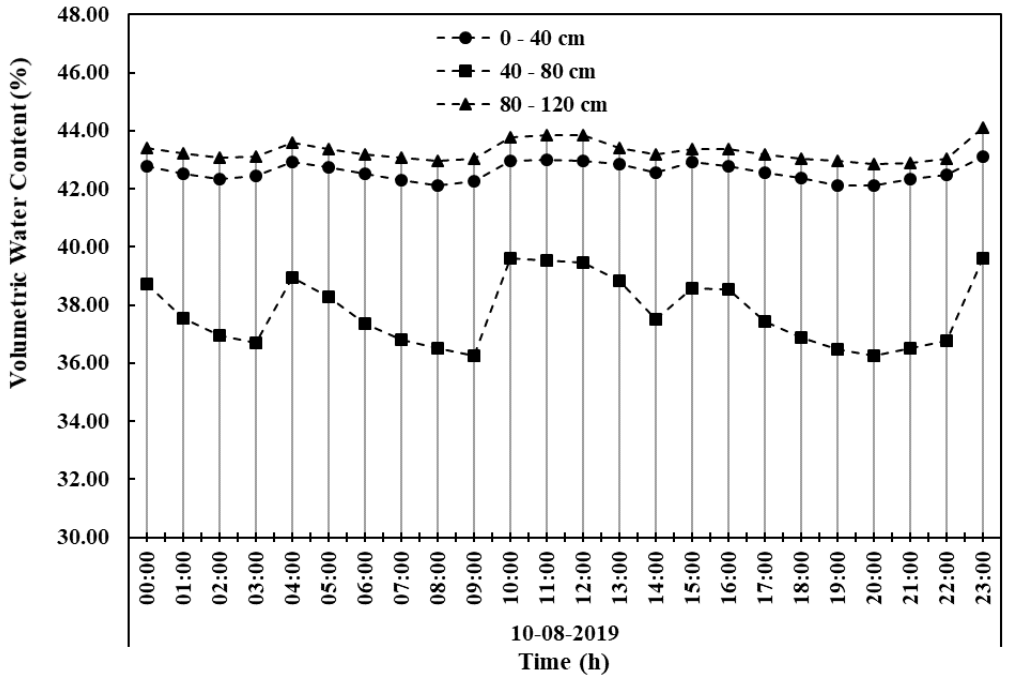

Figure 4.18 Soil moisture data of trench face for 10-08-2019

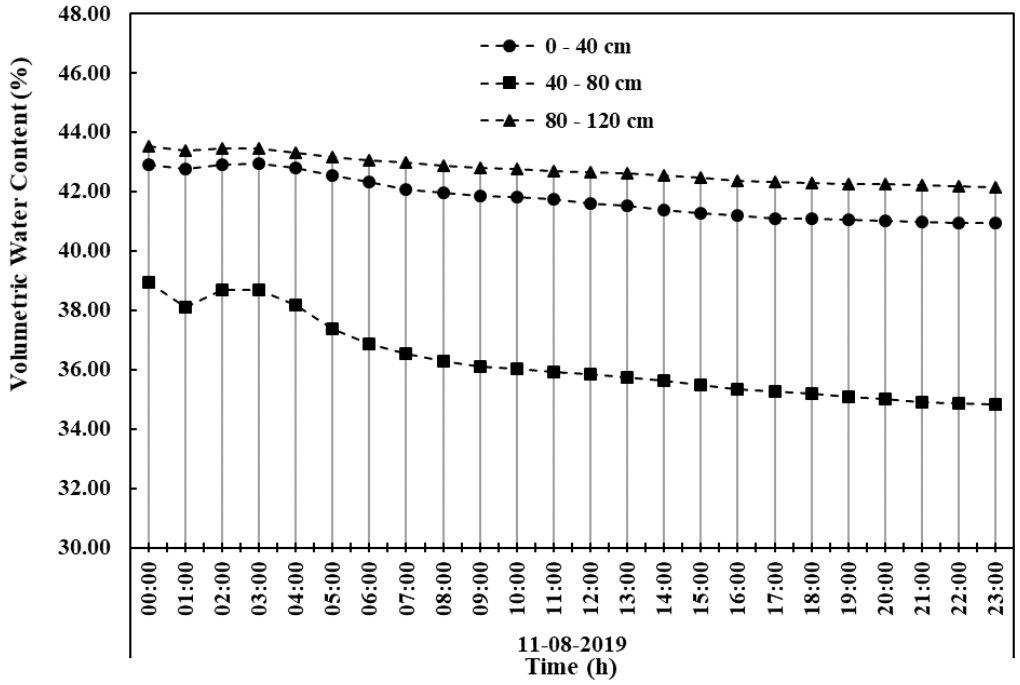

Figure 4.19 Soil moisture data of trench face for 11-08-2019

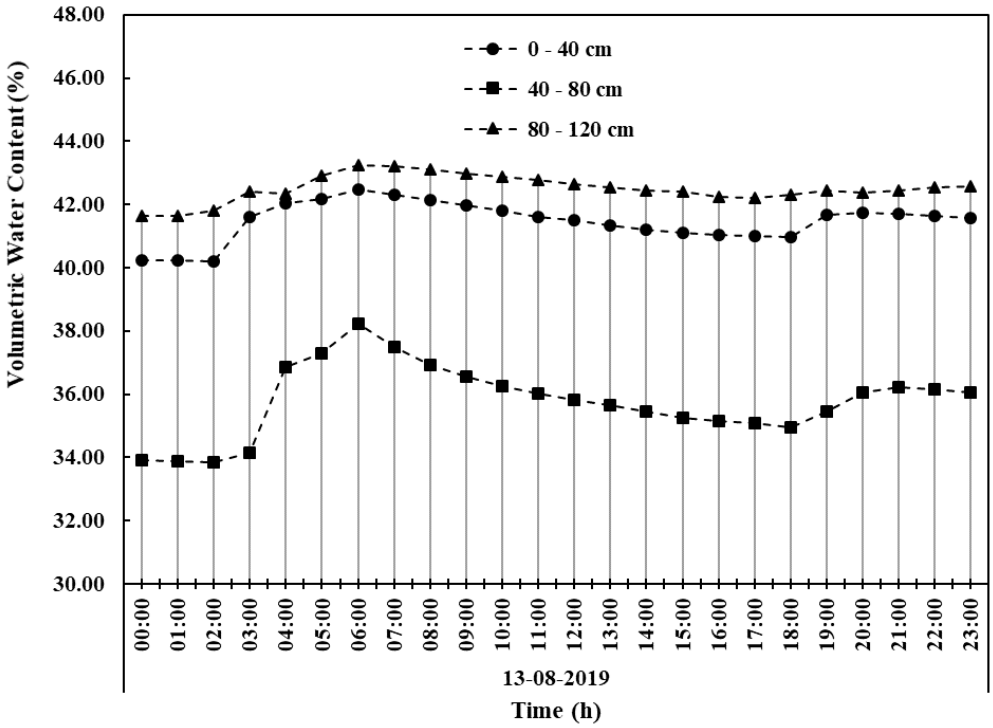

Figure 4.20 Soil moisture data of trench face for 13-08-2019

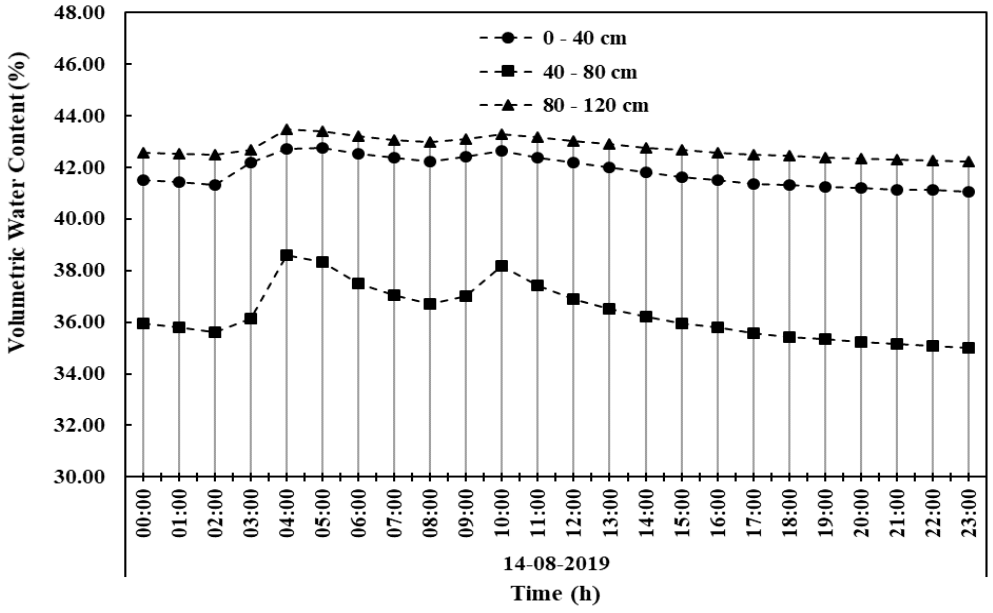

Figure 4.21 Soil moisture data of trench face for 14-08-2019

After analysing the volumetric water content variations from the soil moisture data of the trench face from 31 July 2019 to 14 August 2019, the increase in

volumetric moisture content is converted to the amount of water entered into the soil matrix as subsurface stormflow. Since the considerable increase in the volumetric water content was noticed after a number of rainfall events nearly saturating the soil matrix, the flow could be considered as matrix flow. There was a total of 298 mm rainfall occurred from 31 July 2019 to 14 August 2019. The subsurface stormflow discharge through the first, second and third 40 cm layers of the soil were 24.57 l m^{-2} day^{-1}, 52.74 l m^{-2} day^{-1} and 19.41 l m^{-2} day^{-1} respectively and the subsurface stormflow through respective depths of soil as a percentage of total subsurface stormflow were calculated to be 25.40 %, 54.53 % and 20.07 %. From this study the velocity of subsurface stormflow through the three depths were calculated using the Equation 3.5. The subsurface stormflow velocities through 0-40 cm, 40-80 cm and 80-120 cm soil layers were 23.74 cm day^{-1}, 36.23 cm day^{-1} and 17.41 cm day^{-1} respectively.

4.3.4.1 Discharge versus daily rainfall depth graph for experimental setup 3

The graph between daily subsurface stormflow discharge and the daily rainfall depth for the days of the experiment for experimental setup 3 has been shown in figure 4.22.

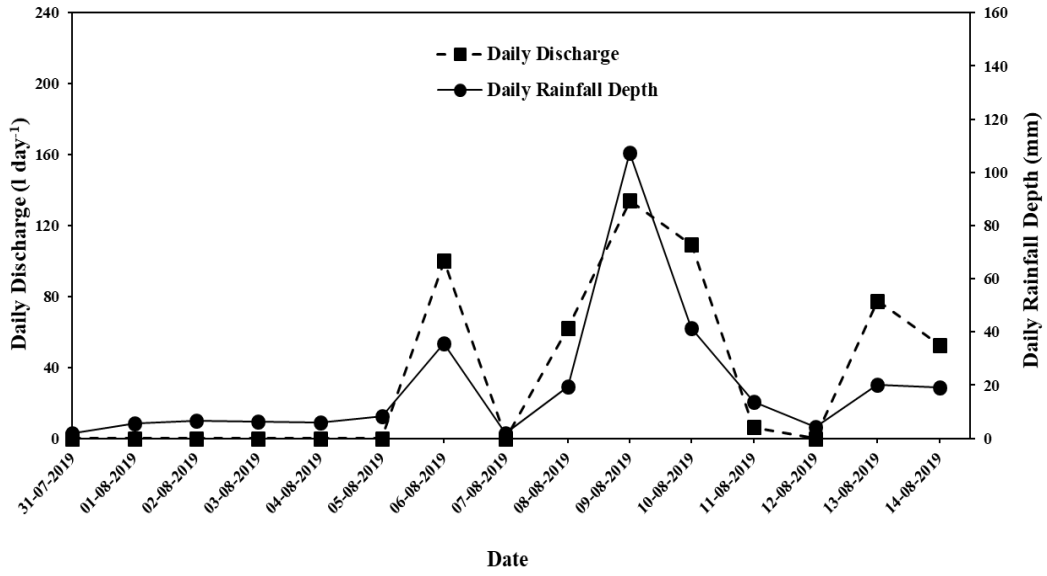

Figure 4.22 Subsurface stormflow discharge versus daily rainfall depth graph

After analysing the graph between daily subsurface stormflow discharge and the daily rainfall depth for the days of the experiment for experimental setup 3, it is clear that the days with high values of rainfall exhibited high discharge of subsurface stormflow. There exists a positive correlation between the daily rainfall depth and daily subsurface stormflow discharge.

4.3.4.2 Discharge versus time graph for experimental setup 3

The plotted graphs between subsurface stormflow discharge through unit area of the soil layers and time for the days of the experiment for the experimental setup 3 are given in the figures from figure 4.23 to figure 4.26.

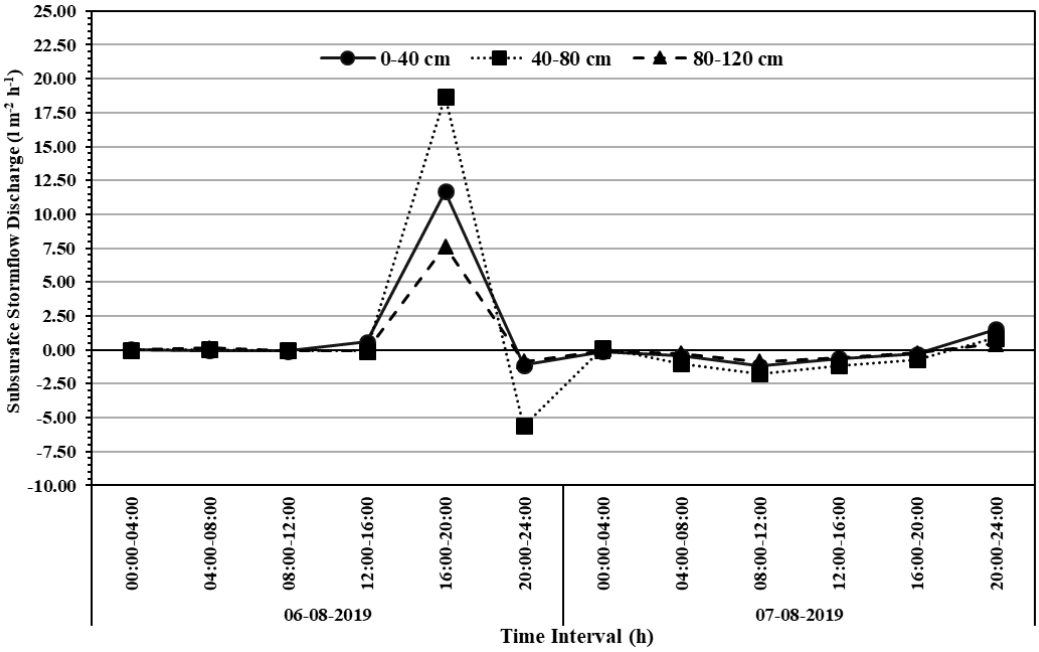

Figure 4.23 Subsurface stormflow discharge versus time graph of experimental setup 3 for 06-08-2019 and 07-08-2019

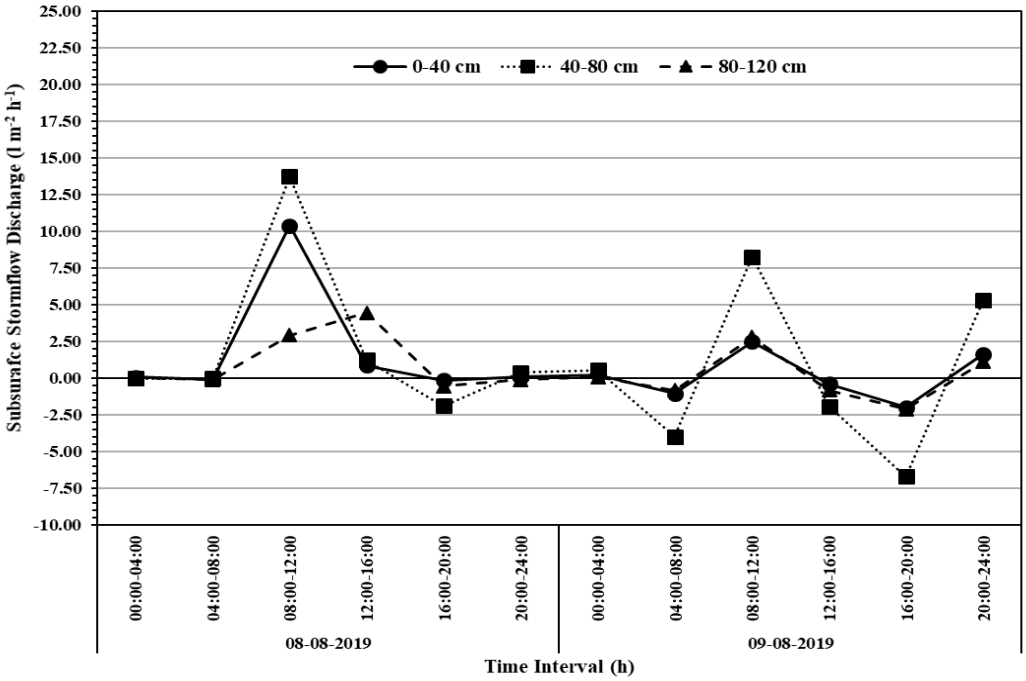

Figure 4.24 Subsurface stormflow discharge versus time graph of experimental setup 3 for 08-08-2019 and 09-08-2019

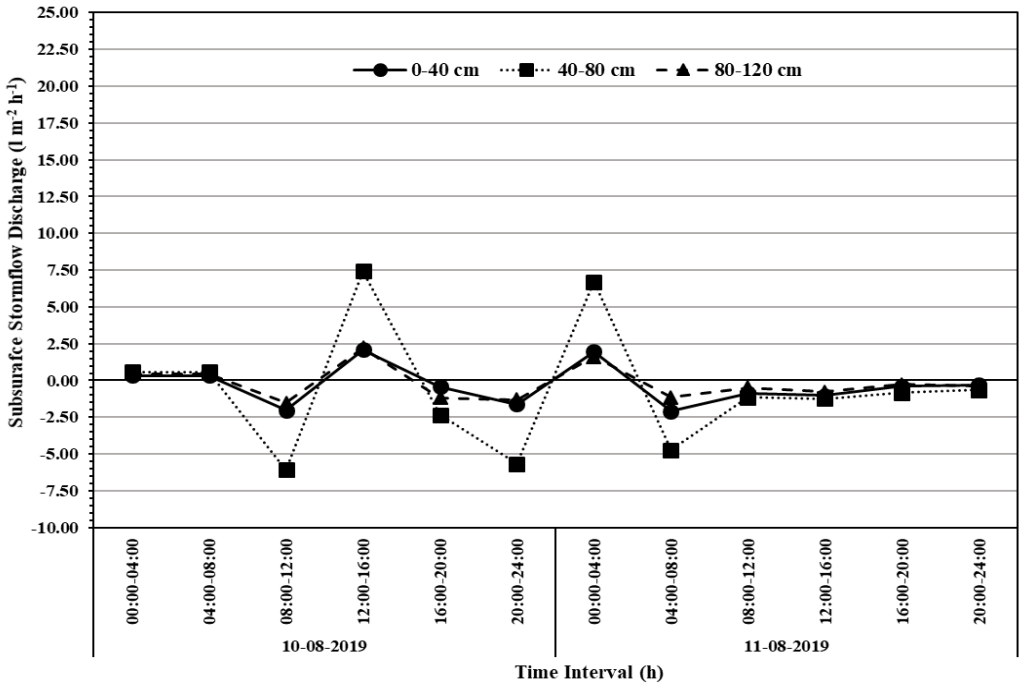

Figure 4.25 Subsurface stormflow discharge versus time graph of experimental setup 3 for 10-08-2019 and 11-08-2019

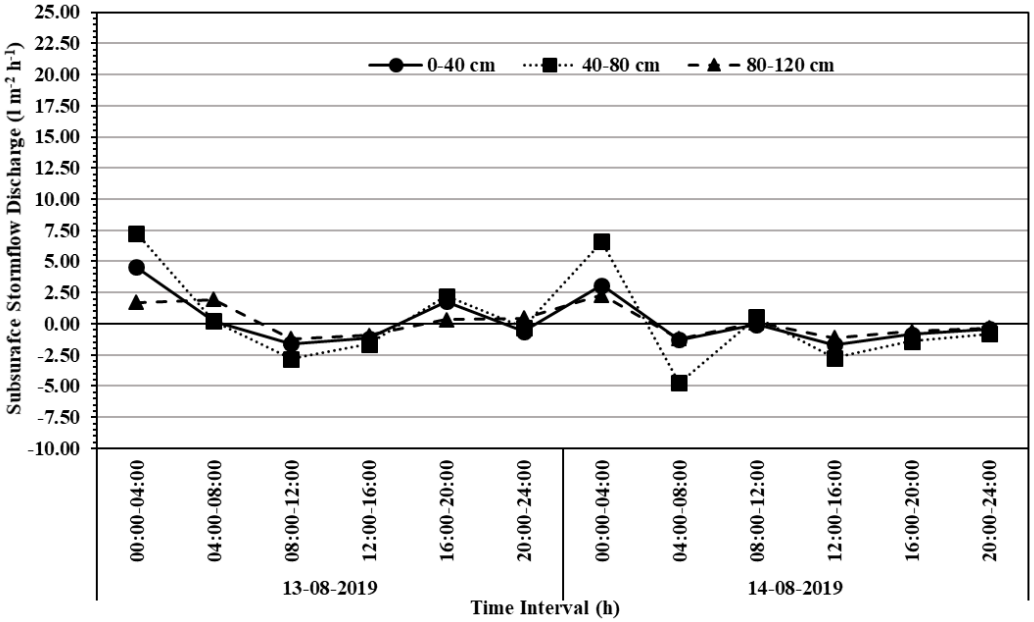

Figure 4.26 Subsurface stormflow discharge versus time graph of experimental setup 3 for 13-08-2019 and 14-08-2019

The subsurface stormflow discharge per unit area of the 40-80 cm soil layer in the second experimental site was found to be maximum for the experimental setup 3. The negative discharge was also maximum for this layer. This is because the variation in moisture content was faster in this layer.

4.3.5 Subsurface Stormflow Discharge Versus Dry Density

Graphs are plotted with the average daily subsurface stormflow discharges and soil dry densities for the different experimental setups which are shown in figure 4.27, figure 4.28 and figure 4.29.

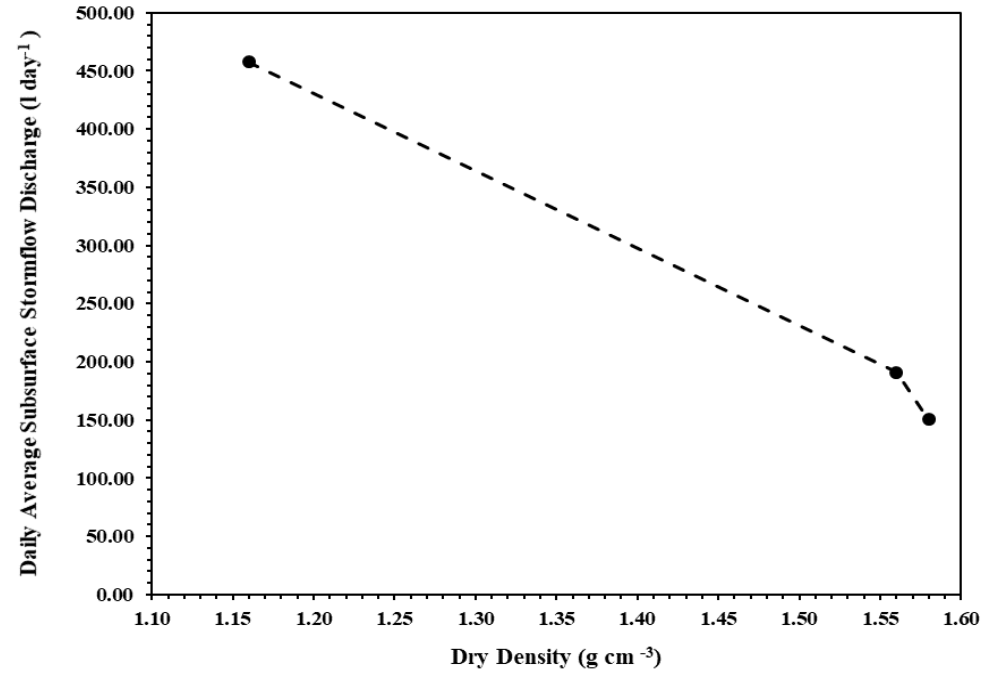

Figure 4.27 Subsurface stormflow discharge versus dry density graph for experimental setup 1

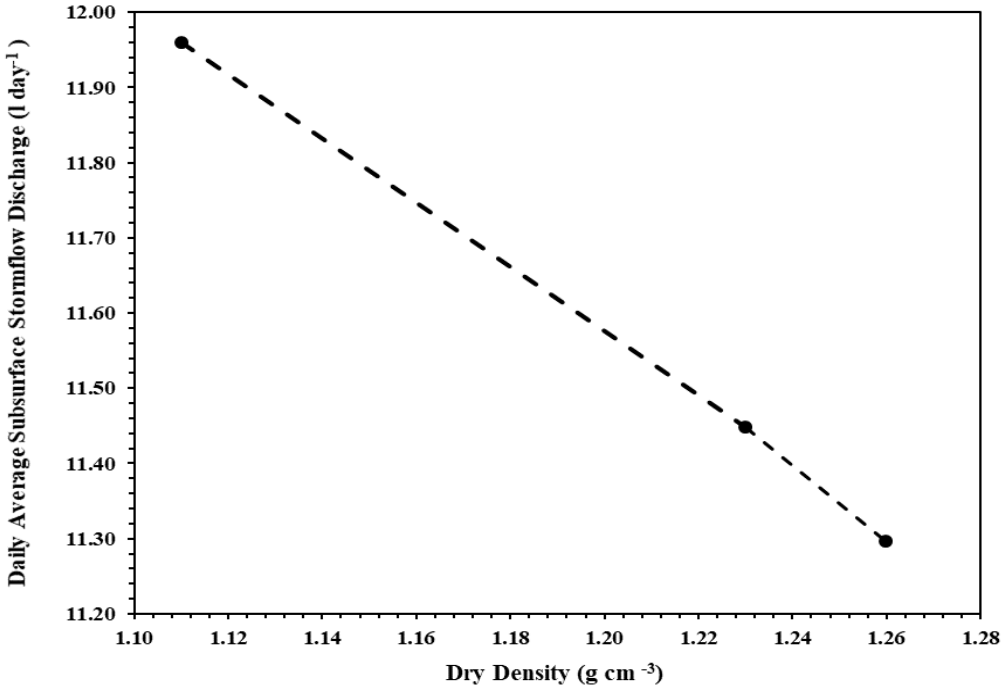

Figure 4.28 Subsurface stormflow discharge versus dry density graph for experimental setup 2

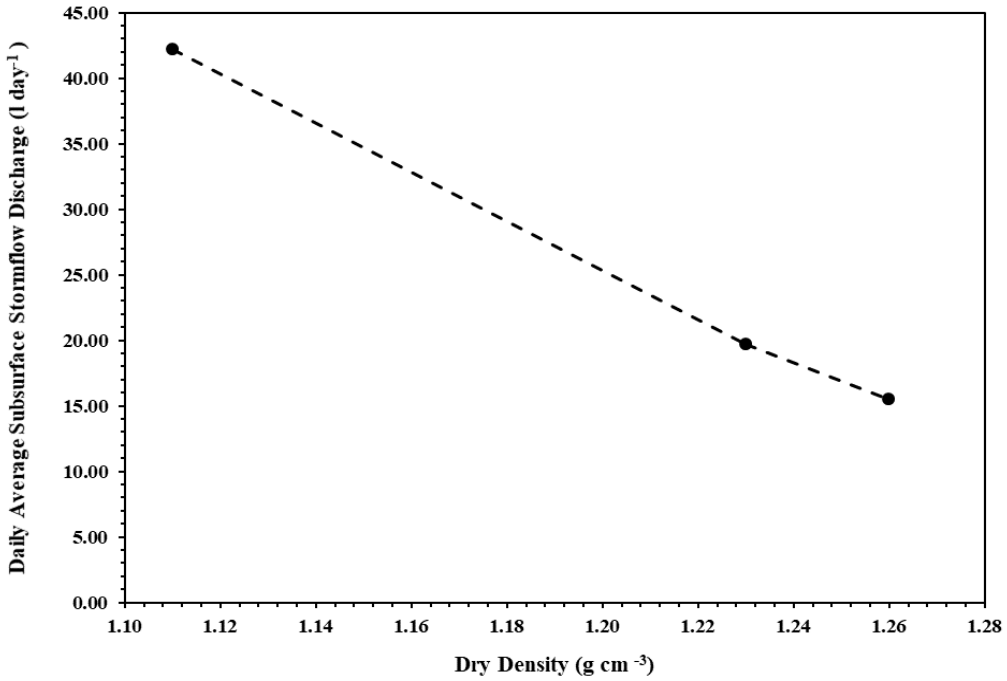

Figure 4.29 Subsurface stormflow discharge versus dry density graph for experimental setup 3

The calculated daily average subsurface stormflow discharge for the three experimental setups clearly shows that the subsurface stormflow discharge and the bulk density of the soil matrix are negatively correlated. This is because more the value of dry density, more will be the suction potential which opposes the water discharge through the soil matrix. Thus the soil matrix having less value of dry density discharges more water as subsurface stormflow compared to the soil matrix with high value of dry density. In the experimental setup 1, the soil layer 0-40 cm discharges more amount of water as subsurface stormflow (457.82 l day^{-1}), followed by the next two layers 40-80 cm and 80-120 cm with discharge of 190.82 l day^{-1} and 150.43 l day^{-1} respectively. For the experimental setups 2 and 3 the maximum subsurface stormflow discharge was found through 40-80 cm depth because the two experimental setups were in the second site where the 40-80 cm soil layer was having the minimum value of dry density compared to the other two depths. These results are tabulated in table 4.4.

Table 4.4 Average Daily Subsurface Stormflow Discharge through different depths for the three experimental setups

Experimental setup	Depth (cm)	Dry Density (g cm^{-3})	Subsurface Stormflow Discharge (l m^{-2} day^{-1})
1	0-40	1.16	190.76
	40-80	1.56	79.52
	80-120	1.58	62.68
2	0-40	1.23	11.80
	40-80	1.11	22.80
	80-120	1.26	8.00
3	0-40	1.23	24,57
	40-80	1.11	52.74
	80-120	1.26	19.41

4.4 SOIL SUCTION DATA STUDIES

The variation in the soil suction pressure according to the variation of volumetric water content for the two experimental sites have been studied by fixing tensiometers and TEROS 12 sensors at the trench face for different depths. The tensiometers fixed at three depths gives the soil suction data according to the volumetric moisture content at the corresponding depths obtained with the sensors. The soil suction variation according to the volumetric water content for the two experimental sites are tabulated in table 4.5 and table 4.6.

Table 4.5 Variation of soil suction with variation in volumetric water content for the first experimental site

Depth (cm)	Soil Suction (kPa)	Volumetric Moisture Content (%)
0-40	6	35.64
	10	31.47
	12	30.26
	15	29.98
	18	28.86
	20	28.20
	26	27.14
40-80	6	37.28
	10	33.11
	12	31.90
	13	31.62
	15	30.50
	18	29.84
	20	28.78
80-120	8	38.25
	10	34.08
	12	32.87
	14	32.59
	15	31.47
	17	30.81
	19	29.75

Table 4.6 Variation of soil suction with variation in volumetric water content for the second experimental site

Depth (cm)	Soil Suction (kPa)	Volumetric Moisture Content (%)
0-40	11	34.91
	16	30.74
	20	29.53
	23	29.25
	25	28.13
	27	27.47
	30	26.41
40-80	10	31.34
	15	27.17
	17	25.96
	22	25.68
	23	24.56
	26	23.90
	27	22.84
80-120	12	35.23
	18	31.06
	23	29.85
	26	29.57
	28	28.45
	29	27.79
	32	26.73

From the soil suction variation data in accordance with volumetric water content, soil water characteristic curves for the two experimental sites are obtained and is shown in figure 4.30 and figure 4.31.

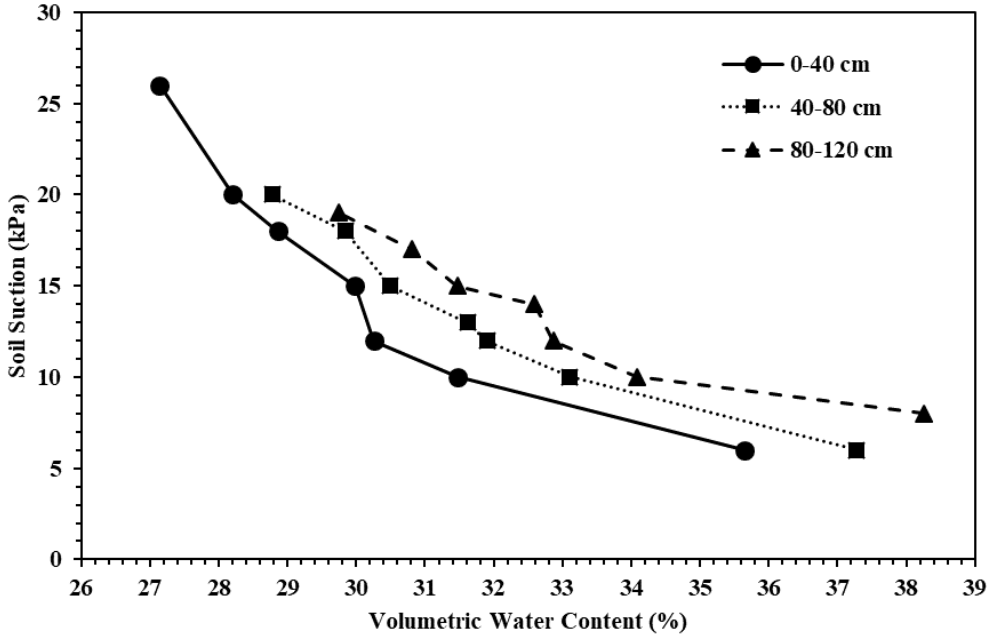

Figure 4.30 Soil water characteristic curve for the first experimental site

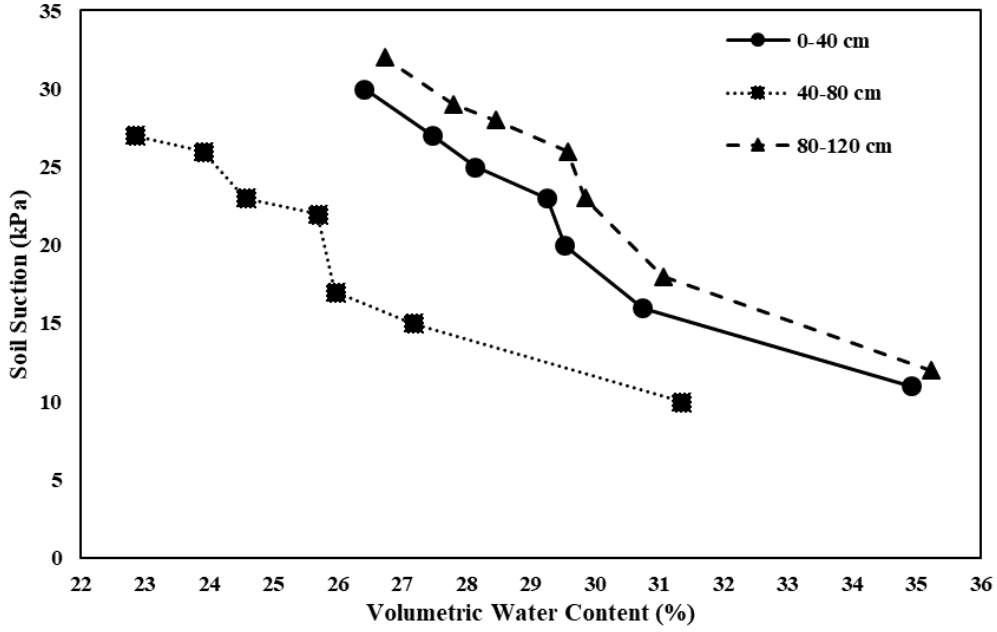

Figure 4.31 Soil water characteristic curve for the second experimental site

From the soil water characteristic curve for the first site, it is found that, for the same moisture content the soil suction was maximum for the depth 80-120 cm which was having high value of dry density (1.58 g cm^{-3}) followed by the depths

40-80 cm and 0-40 cm having dry density values of 1.56 g cm^{-3} and 1.16 g cm^{-3} respectively. Therefore, for the first experimental site, the values of soil suction and the soil dry density are positively correlated.

For the second experimental site the dry density was found minimum at 40-80 cm depth (1.11 g cm^{-3}) and maximum for 80-120 cm depth (1.26 g cm^{-3}). From the soil water characteristic curve obtained for the second site, it is evident that, for the same moisture content the soil suction was found minimum for 40-80 cm depth. Therefore, for the second experimental site, the soil suction values and the soil dry density values are positively correlated. For both the experimental sites, the soil suction and soil dry density are having a positive correlation between them. Hence the soil moisture suction increase with the increase in the soil dry density for the same moisture content. This is because the unit volume of the soil matrix with high dry density will have more soil particles for the suction of water particles compared to the unit volume of soil matrix with a lesser dry density.

4.5 APPLICATION OF TRACER

For determining the velocity of subsurface stormflow through different depths, 120 ppm of sodium chloride solution is applied to the shallow trench prepared 2 m upslope to the through-flow trench at the second experimental site by filling the shallow trench with the tracer solution four times a day *i.e.* 45 l of the sodium chloride solution is applied to the shallow trench at 6 am, 10 am, 2 pm and 6 pm in each day until a noticeable increase in the value of EC is detected by the TEROS 12 sensors fixed at the three depths on the trench face. The background EC value is also determined using the sensor. The background EC for the prepared sodium chloride solution was 0.2210 mS cm^{-1}. The breakthrough curve for the tracer application is obtained for the trench face and is shown in figure 4.32.

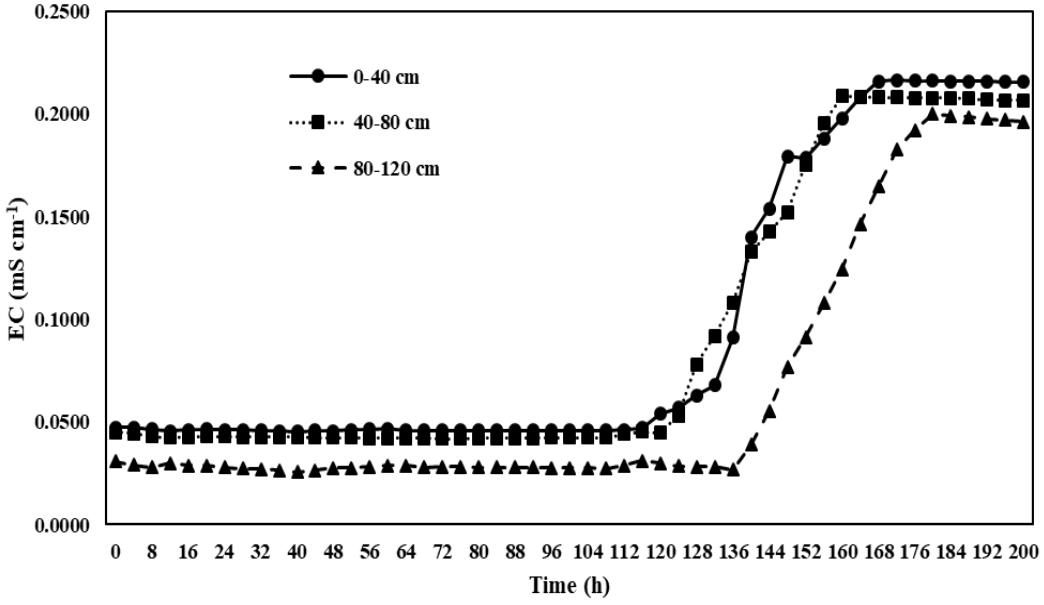

Figure 4.32 Tracer breakthrough curve for the trench face for different depths

By analysing the tracer breakthrough curve it was found that the peak values of EC for the depths 0-40 cm, 40-80 cm and 80-120 cm were obtained after 176 h, 160 h and 180 h respectively after the tracer application, therefore the velocity of subsurface stormflow through the depths 0-40 cm, 40-80 cm and 80-120 cm are calculated to be 27.27 cm day^{-1}, 30 cm day^{-1} and 26.67 cm day^{-1} respectively and the same calculated from the soil moisture studies in the experimental setup 3 were 23.74 cm day^{-1}, 36.23 cm day^{-1} and 17.41 cm day^{-1} respectively. For both the cases the subsurface stormflow velocity was maximum for the 40-80 cm deep soil layer of the second experimental site. This is because 40-80 cm soil layer was having the least value of dry density and hence the soil suction which restricts the fluid flow through an unsaturated soil medium is minimum. The subsurface stormflow velocity versus dry density graph is plotted and is shown in Figure 4.33.

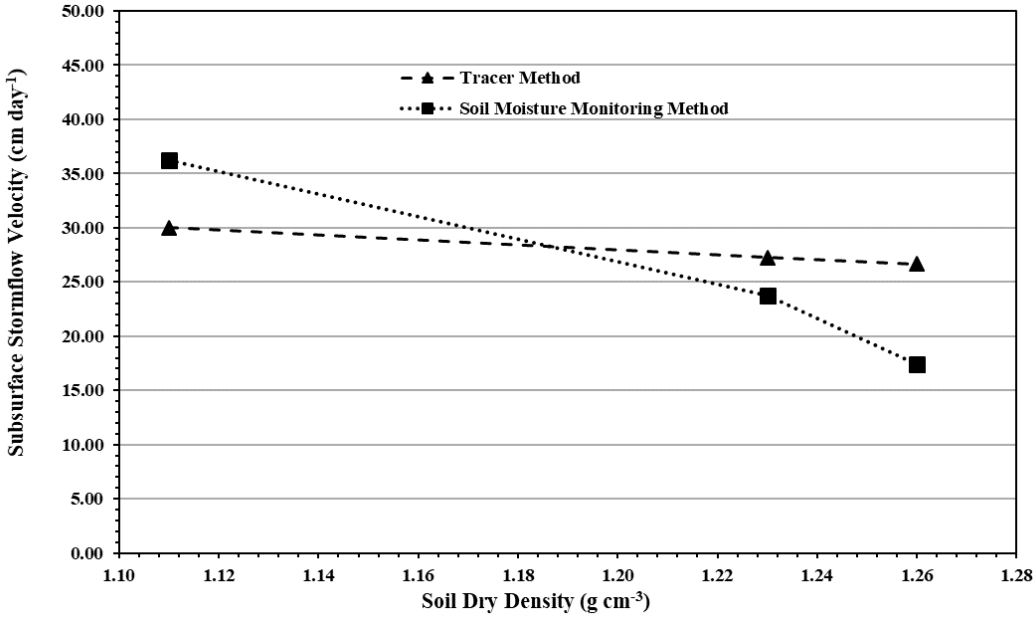

Figure 4.33 Subsurface stormflow velocity versus dry density graph

From the Figure 4.33 it is evident that the velocity of subsurface stormflow and the soil dry density are negatively correlated for both the experimental methods. This is because the soil layer having a high value of dry density will have greater number of soil particles compared to the soil layer having less dry density. Therefore, the suction potential will be more on the former case than the latter. The pressure needed for initiating the fluid flow through the dense soil is more than that of light soil and hence the velocity of subsurface stormflow will be higher for the latter.

A graph between subsurface stormflow velocities through different depths of soil and the respective void ratios is shown in figure 4.34 for the second experimental site using tracer method and soil moisture monitoring method.

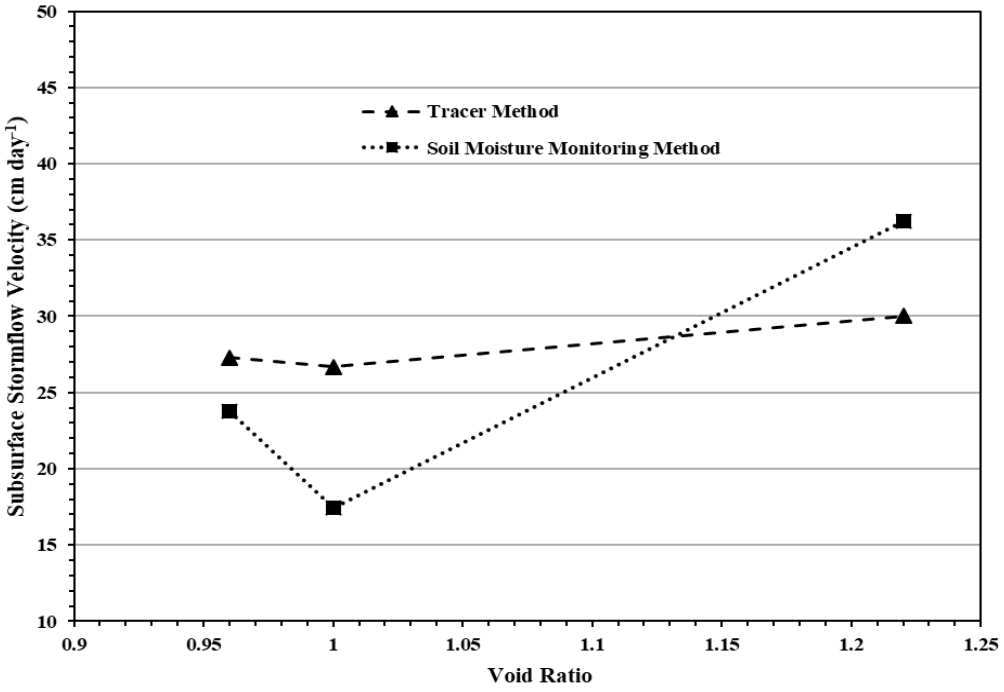

Figure 4.34 Subsurface Stormflow velocity versus void ratio graph for second experimental site

The subsurface flow velocity through the 40-80 cm deep soil layer which is having higher void ratio than the other two layers is higher compared to the 0-40 cm and 80-120 cm deep layers. This is because the soil suction for 40-80 cm is the lowest among the three layers at a specific time and the moisture in this layer is more easily drained out as subsurface stormflow. As a result, the moisture content in this layer is found to be less. The volume of air in this layer is high and it makes the void ratio higher for the 40-80 cm layer. In case of the third layer (80-120 cm), it exhibits high soil suction among the three layers. Therefore, the subsurface stormflow velocity through this layer exhibits the smallest value and the moisture content for this layer exhibits high values. For the 0-40 cm layer, the soil suction is higher than 40-80 cm layer and lower than the 80-120 cm layer. Thus the moisture content of 0-40 cm layer is higher than that of 40-80 cm layer and lesser then that of 80-120 cm layer. The void ratio of 0-40 cm layer is lower than 80-120 cm layer because of the less volume of water in 0-40 cm layer due to less moisture content than 80-120 cm layer.

SUMMARY AND CONCLUSION

CHAPTER V

SUMMARY AND CONCLUSION

Water conservation assumes great significance in most part of the world to solve water scarcity in a sustainable way. Water shortage is experienced even in high annual rainfall areas with high infiltration bearing top soil. The state of Kerala in India is a typical example for the same. To plan water conservation in a scientific manner, the pathways of water movement after the rain hit on the land terrain need to be understood. Rain water moves out from a land terrain in three principal ways *i.e.* surface runoff, lateral flow and baseflow. A quantified knowledge on all the three component processes is a must to plan appropriate water conservation interventions.

Studies related to the subsurface stormflow process are very restricted due to the complexity of the process and difficulty of its observation. The study entitled "Determination of subsurface stormflow using tracer method" has envisioned to throw more insight into the phenomenon of subsurface stormflow. For the observation purpose, two experimental plots from KCAET campus, Kerala, India were used with three experimental setups. The sites were situated at 10^{o} 51'18" N latitude and 75^{o} 59'11" E longitude at an altitude of 10 m above mean sea level.

The experimental setup 1 was framed on the first site. A through-flow trench of length 6 m, width 0.6 m and depth 1.8 m has been excavated on the first site at the downstream end. For simulating the rainfall, a butterfly sprinkler was fixed at the centre of the plot, 8 m upslope from the through-flow trench. The sprinkler was operated 12 hours a day, from 6 am to 6 pm. The through-flow trench face was divided into three depths, *i.e.* 0 to 40 cm, 40 to 80 cm and 80 to 120 cm for determining the spatial variation in the subsurface stormflow throughout the trench profile. The subsurface stormflow through the soil matrix is studied by soil moisture data gravimetrically. It was found that 13.21 % of the total applied water has been lost as the subsurface storm flow. The quantity of subsurface stormflow, as percentage of the applied water to the experimental setup 1, through vertical profiles

of 0-40 cm, 40-80 cm and 80-120 cm were 7.57 %, 3.16 % and 2.49 % respectively. The Subsurface stormflow discharge through these three depths were 190.76 l m^{-2} day^{-1}, 79.52 l m^{-2} day^{-1} and 62.68 l m^{-2} day^{-1} respectively

The experimental setup 2 has been formed by excavating a through-flow trench of 3 m length, 0.6 m width and 1.5 m depth on the second plot in order to intersect the subsurface flow. A shallow trench of length 2 m, width 0.3 m and 0.3 m depth which is constructed 4 m upslope to the through flow trench. The procedure for the study in the experimental setup 2 was the line application of water to the shallow trench upslope to the through-flow trench frequently for a consecutive 10 days. Water infiltrated from the trench is replenished regularly. The infiltrated water is expected to flow towards the through-flow trench. The through-flow trench face was divided into three profiles, *i.e.* 0 to 40 cm, 40 to 80 cm and 80 to 120 cm for determining the spatial variation in the subsurface stormflow through soil moisture observations. The soil moisture at the trench face is observed at predefined intervals after the line application of water into the shallow trench. Observations at the experimental setup 2 was continued for 10 days. It did make only little variation in the volumetric water content on the trench face. A total of 7428 l water has applied to the shallow trench from Day 1 to Day 10. The subsurface flow occurred during these days was observed to be only 4.67 % of the total line application of water. So, there was no considerable preferential connectivity between the line application of water and the trench face in experimental setup 2. The percentage of applied water as subsurface stormflow through the depths 0-40 cm, 40-80 cm and 80-120 cm were 1.54 %, 1.61 % and 1.52 % respectively. The subsurface stormflow discharges through 0-40 cm, 40-80 cm and 80-120 cm depths were found as 11.80 l m^{-2} day^{-1}, 22.80 l m^{-2} day^{-1} and 8.00 l m^{-2} day^{-1} respectively.

In the monsoon season the experimental setup 2 on the second plot has converted to experimental setup 3 by making use of the natural rainfall input. A shallow trench for deviating the surface runoff from the upslope areas of the observation trench was constructed. The through flow trench as well as an area to 1 m upslope of the through-flow trench was covered using a tarpaulin sheet for

restricting the entry of direct rainfall to the through-flow trench. The through-flow trench face was divided into three depths for determining the spatial variation in the subsurface stormflow throughout the trench face the same way as that of experimental setup 2. The soil moisture measurements were done at the trench face for these depths for a consecutive 15 days with rainfall. The soil moisture and EC studies were carried out using TEROS 12 capacitive sensors and ZL6 data logger for experimental setup 3. The three sensors were calibrated for the three depths and the calibrated functions were updated in the "zentra cloud". The subsurface stormflow discharge through the first, second and third 40 cm depths of the soil were found to be 24.57 l m^{-2} day^{-1}, 52.74 l m^{-2} day^{-1} and 19.41 l m^{-2} day^{-1} respectively and these flows as percentages of total subsurface stormflow were 25.40 %, 54.53 % and 20.07 %. The subsurface stormflow velocities through 0-40 cm, 40-80 cm and 80-120 cm soil layers were 23.74 cm day^{-1}, 36.23 cm day^{-1} and 17.41 cm day^{-1} respectively.

The soil water characteristics curves were obtained for the three depths for the two experimental sites from the data obtained for the soil moisture sensors and the tensiometers fixed at the corresponding three depths. It was found that the dry density of soil and the soil moisture suction are positively correlated.

In order to obtain the subsurface stormflow velocities through different depths of the soil tracer application was done using 120 ppm sodium chloride solution as tracer. A shallow trench of length 0.5 m, width 0.3 m and depth 0.3 m was constructed 2 m upslope to the through-flow trench at the second site. The tracer solution was applied regularly to the shallow trench until the sensors fixed to the trench face detects the hike in the EC value which will indicates the entry of subsurface stormflow to the trench. From the tracer experiment the velocities of subsurface stormflow through the depths 0-40 cm, 40-80 cm and 80-120 cm were calculated as 27.27 cm day^{-1}, 30.00 cm day^{-1} and 26.67 cm day^{-1} respectively.

From all the experiments and observations, the following conclusions were made;

1. There exists a positive correlation between the soil dry density and the soil suction potential.
2. The subsurface stormflow discharge through the soil matrix was found to vary significantly with variation in soil dry density. This is because the increase in dry density will decrease the proportion of macro pores and will increase the soil suction potential and both of these effects will hinder the flow through the soil matrix.
3. The velocity of subsurface stormflow through the soil layer having less dry density will be higher than the velocity of subsurface stormflow through the soil layer having higher dry density.
4. The subsurface stormflow contribution in the experimental setup 2 with line application of water and having a land slope of 8 % was only 4.67 % of the total applied water. This result indicates that major portion of the applied water in concentrated form goes as deep percolation.
5. In experimental setups 1 and 3, where the water input was from simulated rainfall and natural rainfall, considerable discharges of subsurface stormflow were obtained. This indicates that subsurface flow depends on the nature of application of water on the soil surface. Significant variation in subsurface stormflow quantity resulting from different types of application of water on the soil surface was observed.
6. The rainfall intensity along with the soil physical properties were also found to affect the subsurface stormflow discharge as a percentage of total applied water.
7. In all the experimental setups the major portion of the subsurface stormflow was through the first 80 cm soil layer. It was also found from the experimental setup 2 that the subsurface stormflow becomes considerably less when the water is forced to infiltrate through the shallow trench of line application. So by providing the ground water recharge methods such as rain pits beyond 80 cm depth can considerably reduce the quantity of subsurface stormflow.

REFERENCES

CHAPTER VI

REFERENCES

Ahuja, L.R. and Lehman, O.R. 1985. Interflow of water and tracer chemical on sloping field plots with exposed seepage faces. *J. Hydrol*. 76: 307-317.

Ahuja, L.R. and Ross, J.D. 1983. Effect of subsoil conductivity and thickness on inter- flow pathways, rates and source areas for chemicals in a sloping layered soil with seepage face. *J. Hydrol*. 64: 184-204.

Anderson, M.G. and Burt, T.P. 1990. Subsurface runoff. *Process studies in hillslope hydrology*, pp.365-400.

Beven, K. and Germann, P. 1981. Water flow in soil macropores II. A combined flow model. *Journal of Soil Science* 32(1): 15-29.

Beven, K. and Germann, P. 1982. Macropores and water flow in soils. *Water resources research* 18(5): 1311-1325.

Bosch, D.D., Arnold, J.G., Allen, P.G., Lim, K.J., and Park, Y.S. 2017. Temporal variations in baseflow for the Little River experimental watershed in South Georgia, USA. *J. Hydrol*. 10:110-121.

Freer, J., McDonnell, J.J., Beven, K.J., Peters, N.E., Burns, D.A., Hooper, R.P., Aulenbach, B. and Kendall, C. 2002. The role of bedrock topography on subsurface storm flow. *Water Resources Research* 38(12), 1269p.

Germann, P. and Beven, K. 1981. Water flow in soil macropores I. An experimental approach. *Journal of Soil Science* 32(1): 1-13.

Graham, C.B., Woods, R.A. and McDonnell, J.J., 2010. Hillslope threshold response to rainfall:(1) A field based forensic approach. *Journal of Hydrology* 393(1-2): 65-76.

Guo, L., Chen, J. and Lin, H. 2014. Subsurface lateral preferential flow network revealed by time-lapse ground-penetrating radar in a hillslope. *Water Resour. Res.* 50(12): 9127-9147.

Hewlett, J.D. and Hibbert, A.R. 1963. Moisture and energy conditions within a sloping soil mass during drainage. *Journal of geophysical research 68*(4): 1081-1087.

Hewlett, J.D. and Hibbert, A.R., 1967. Factors affecting the response of small watersheds to precipitation in humid areas. *Forest hydrol.* 1: 275-290.

Holden, J. 2004. Hydrological connectivity of soil pipes determined by ground-penetrating radar tracer detection. *Earth Surf. Process. Landforms* 29(4): 437-442.

Hoover, M.D. and Hursh, C.R. 1943. Influence of topography and soil-depth on runoff from forest land. *Eos. Trans. AGU. 24*(2): 693-698.

Horton, R.E. 1933. The role of infiltration in the hydrologic cycle. *Eos. Trans. AGU.* 14(1): 446-460.

Hursh, C.R. 1936. Storm water and absorption. *Eos. Trans. AGU. 17*(2): 301-302.

Hursh, C.R. and Brater, E.F. 1941. Separating storm-hydrographs from small drainage-areas into surface-and subsurface-flow. *Eos. Trans. AGU. 22*(3): 863-871.

Knöll, P. and Scheytt, T. 2018. A tracer test to determine a hydraulic connection between the Lauchert and Danube karst catchments (Swabian Alb, Germany). *Hydrogeol J*. 26(2): 429-437.

Kumar, A., Kanwar, R.S. and Hallberg, G.R. 1997. Separating preferential and matrix flows using subsurface tile flow data. *J. Environ. Sci. Health* A32(6): 1711-1729.

Laudon, H., Hemond, H.F., Krouse, R. and Bishop, K.H. 2002. Oxygen 18 fractionation during snowmelt: Implications for spring flood hydrograph separation. *Water Resources Research* 38(11): 40-1-40-10.

Leibundgut, C. and Seibert, J. 2011. Tracer Hydrology. *Treatise on Water Science* 2: 215–236.

Luo, L., Lin, H. and Halleck, P. 2008. Quantifying soil structure and preferential flow in intact soil using X-ray computed tomography. *Soil Sci. Soc. Am. J.* 72:1058-1069

McDonnell, J.J. 1990. A rationale for old water discharge through macropores in a steep, humid catchment. *Water Resources Research*, 26(11): 2821-2832.

McDonnell, J.J., Owens, I.F. and Stewart, M.K. 1991. A case study of shallow flow paths in a steep zero-order basin. *Journal of the American Water Resources Association* 27(4): 679-685.

Mosley, M.P. 1979. Streamflow generation in a forested watershed, New Zealand. *Water Resources Research* 15(4): 795-806.

Mosley, M.P. 1982. Subsurface flow velocities through selected forest soils, South Island, New Zealand. *J. Hydrol*. 55(1-4): 65-92.

Oberdorster, C., Vanderborght, J., Kemna, A. and Vereecken, H. 2010. Investigating preferential flow processes in a forest soil using time domain reflectometry and electrical resistivity tomography. *Vadose Zone J.* 9(2): 350-361.

Pearce, A.J., Stewart, M.K. and Sklash, M.G. 1986. Storm runoff generation in humid headwater catchments: 1. Where does the water come from?. *Water Resources Research* 22(8): 1263-1272.

Pierret, A., Capowiez, Y., Belzunces, L. and Moran, C.J. 2002. 3D reconstruction and quantification of macropores using X-ray computed tomography and image analysis. *Geoderma*, 106(3-4): 247-271.

Pinder, G.F. and Jones, J.F. 1969. Determination of the ground-water component of peak discharge from the chemistry of total runoff. *Water Resources Research* 5(2): 438-445.

Rawls, W.J., Brakensiek, D.L. and Logsdon, S.D. 1993. Predicting saturated hydraulic conductivity utilizing fractal principles. *Soil Science Society of America Journal* 57(5): 1193-1197.

Richards, K.S. and Reddy, K.R. 2007. Critical appraisal of piping phenomena in earth dams. *Bull. Eng. Geol. Environ.* 66(4): 381-402.

Rodhe, A. 1981. Spring Flood Meltwater or Groundwater? Paper presented at the Nordic Hydrological Conference (Vemdalen, Sweden, August, 1980). *Hydrology Research* 12(1): 21-30.

Sathian, K.K. and Symala, P. 2009. Calibration and validation of a distributed watershed hydrolic model. *Indian J. of Soil Cons.* 37(2): 100-105.

Singh, B. and O'llaghan J.R. 1978. Effect of interflow on soil drainage. *J. agric. Engng Res.* 23: 397-415.

Sklash, M.G., Stewart, M.K. and Pearce, A.J. 1986. Storm runoff generation in humid headwater catchments: 2. A case study of hillslope and low-order stream response. *Water Resources Research* 22(8): 1273-1282.

Skopp, J. 1981. Comment on "micro-, meso-, and macroporosity of soil". *Soil Science Society of America Journal*, 45(6): 1246-1246.

Tani, M. 1997. Runoff generation processes estimated from hydrological observations on a steep forested hillslope with a thin soil layer. *Journal of Hydrology* 200(1-4): 84-109.

Tirumalesh, K., Shivanna, K., Noble, J., Narayan, K. and Xavier, K. 2007. Nuclear techniques to investigate source and origin of groundwater pollutants and their flow path at Indian Rare Earths Ltd., Cochin, Kerala. *Journal of Radioanalytical and Nuclear Chemistry* 274(2): 307-313.

Tromp-van Meerveld, H.J. and McDonnell, J.J. 2006a. Threshold relations in subsurface stormflow: 1. A 147-storm analysis of the Panola hillslope. *Water Resources Research* 42(2), 2410p.

Tromp-van Meerveld, H.J. and McDonnell, J.J., 2006b. Threshold relations in subsurface stormflow: 2. The fill and spill hypothesis. *Water Resources Research* 42(2), 2410p.

Weiler, M., Uchida, T. and McDonnell, J. 2003. Connectivity due to preferential flow controls water flow and solute transport at the hillslope scale. In *Proceedings of MODSIM*.

Whipkey, R.Z. 1965. Subsurface stormflow from forested slopes. *Hydrological Sciences Journal* 10(2): 74-85.

WMO (World Meteorological Organisation) 2012. *International Glossary of Hydrology* (3rd Ed.), World Meteorological Organization, Geneva, 336p.

Zhu, Q., Lin, H. and Doolittle, J. 2010. Repeated electromagnetic induction surveys for improved soil mapping in an agricultural landscape. *Soil Sci. Soc. Am. J.* 74(5): 1763-17

APPENDICES

APPENDICES

APPENDIX I

Soil moisture data of trench face for experimental setup 1

Date	Time	Gravimetric moisture content (%)		
		0-40 cm	40-80 cm	80-120 cm
05-02-2019	06:00	22.66	18.46	23.72
	08:00	22.87	20.06	26.33
	10:00	24.58	20.37	23.74
	12:00	25.29	21.54	24.62
	14:00	22.68	20.55	26.30
	16:00	22.02	19.85	26.79
	18:00	24.60	20.99	27.49
06-02-2019	06:00	21.48	23.28	29.84
	08:00	23.58	23.89	28.95
	10:00	21.98	18.63	25.06
	12:00	20.85	19.50	29.88
	14:00	22.74	23.46	27.33
	16:00	20.99	21.54	23.67
	18:00	22.94	20.79	34.02
07-02-2019	06:00	21.11	17.91	25.72
	08:00	21.21	20.56	25.57
	10:00	23.04	22.58	31.87
	12:00	23.95	22.32	30.66
	14:00	21.79	21.29	23.58
	16:00	24.72	22.75	27.83
	18:00	22.75	23.13	31.97

APPENDIX II

Soil moisture data analysis for experimental setup 1

Date	Depth (cm)	Time	Gravimetric Moisture Content (%)	Increase in Gravimetric Moisture Content (%)	Volume of water (L)	Total Discharger (l day^{-1})	
05-02-2019	0-40	06:00	19.18	2.61	98.97	241.17	524.45
		08:00	21.79				
		10:00	19.20	3.75	142.20		
		18:00	22.95				
	40-80	06:00	23.10	3.08	115.32	158.00	
		12:00	26.18				
		16:00	24.49	1.14	42.68		
		18:00	25.63				
	80-120	06:00	25.33	2.63	53.45	125.28	
		12:00	27.96				
		16:00	24.69	2.58	71.83		
		18:00	27.27				
06-02-2019	0-40	10:00	17.21	4.82	182.77	575.25	911.34
		12:00	22.03				
		16:00	15.82	10.35	392.47		
		18:00	26.17				
	40-80	06:00	25.81	0.61	22.46	170.73	
		08:00	26.42				
		10:00	21.16	4.83	148.26		
		14:00	25.99				
	80-120	06:00	26.47	2.10	58.46	165.37	
		08:00	28.57				
		12:00	25.84	1.89	52.62		
		14:00	27.73				
		16:00	25.98	1.95	54.29		
		18:00	27.93				
07-02-2019	0-40	08:00	20.72	6.30	238.90	557.04	961.42
		10:00	27.02				
		14:00	18.73	8.39	318.15		
		18:00	27.12				
	40-80	06:00	21.11	4.67	174.84	243.73	
		10:00	25.78				
		14:00	24.49	1.84	68.89		
		18:00	26.33				
	80-120	06:00	23.08	2.84	79.07	160.64	
		12:00	25.92				
		14:00	23.76	2.93	81.57		
		16:00	26.69				

APPENDIX III

Soil moisture data of trench face for experimental setup 2

Day	Time (h)	Volumetric Water Content (%)			Volume of Water Applied (L)
		0-40 cm	40-80 cm	80-120 cm	
1	06:00	15.80	15.23	16.81	1248
	10:00	16.27	16.73	16.92	
	14:00	17.20	17.54	17.90	
	18:00	17.01	17.47	17.66	
2	06:00	14.46	13.79	16.11	1440
	10:00	14.93	15.29	16.46	
	14:00	15.70	16.40	16.85	
	18:00	15.67	16.03	16.61	
3	06:00	16.59	16.53	17.89	852
	10:00	16.75	17.18	18.17	
	14:00	17.68	17.99	18.57	
	18:00	17.49	17.92	18.33	
4	06:00	16.56	16.01	17.69	744
	10:00	17.03	17.51	17.80	
	14:00	17.85	18.30	18.65	
	18:00	17.77	18.25	18.54	
5	06:00	15.22	14.57	16.99	732
	10:00	15.69	16.07	17.23	
	14:00	16.46	16.94	17.59	
	18:00	16.43	16.81	17.49	
6	06:00	17.69	16.91	18.77	612
	10:00	18.02	17.96	18.95	
	14:00	18.44	18.77	19.45	
	18:00	18.25	18.70	19.21	
7	06:00	15.37	14.80	16.38	432
	10:00	15.84	16.30	16.49	
	14:00	16.68	17.25	17.47	
	18:00	16.58	17.04	17.23	
8	06:00	14.03	13.36	15.68	480
	10:00	14.50	14.86	15.97	
	14:00	15.26	15.97	16.37	
	18:00	15.24	15.60	16.18	
9	06:00	16.28	15.57	17.53	420
	10:00	16.32	16.75	17.85	
	14:00	17.25	17.56	18.14	
	18:00	17.06	17.49	17.90	
10	06:00	16.13	15.58	17.26	468
	10:00	16.60	17.08	17.37	
	14:00	17.42	17.85	18.16	
	18:00	17.34	17.82	18.11	

APPENDIX IV

Soil moisture data analysis for experimental setup 2

Day	Depth (cm)	Increase in Volumetric Water Content (%)	Discharge (l)
1	**0-40**	1.65	13.20
	40-80	1.53	12.24
	80-120	1.70	13.60
2	**0-40**	1.49	11.92
	40-80	1.83	14.64
	80-120	1.35	10.80
3	**0-40**	1.34	10.72
	40-80	1.21	9.68
	80-120	1.29	10.32
4	**0-40**	1.54	12.32
	40-80	1.51	12.08
	80-120	1.57	12.56
5	**0-40**	1.49	11.92
	40-80	1.59	12.72
	80-120	1.21	9.68
6	**0-40**	1.00	8.00
	40-80	1.08	8.64
	80-120	1.29	10.32
7	**0-40**	1.56	12.48
	40-80	1.67	13.36
	80-120	1.70	13.60
8	**0-40**	1.48	11.84
	40-80	1.83	14.64
	80-120	1.30	10.40
9	**0-40**	1.22	9.76
	40-80	1.21	9.68
	80-120	1.22	9.76
10	**0-40**	1.54	12.32
	40-80	1.49	11.92
	80-120	1.49	11.92

APPENDIX V

TEROS 12 calibration data

(a) Calibration data for sensor 1

Soil + Container Weight (g)		Wet Weight (g)	Water Weight (g)	Gravimetric Water Content (g g^{-1})	Sensor Measurements (RAW)	Volumetric Water Content (m^3 m^{-3})
Air dry	6890.00	6584.00	480.08	0.09	1974.00	0.09
Point 2	7423.00	7117.00	1013.08	0.19	2083.50	0.19
Point 3	7925.60	7619.60	1515.68	0.29	2255.70	0.29
Point 4	8398.00	8092.00	1988.08	0.37	2660.20	0.37
Point 5	8837.00	8531.00	2427.08	0.46	2924.40	0.46

(b) Calibration data for sensor 2

Soil + Container Weight (g)		Wet Weight (g)	Water Weight (g)	Gravimetric Water Content (g g^{-1})	Sensor Measurements (RAW)	Volumetric Water Content (m^3 m^{-3})
Air dry	6572.40	6266.40	748.23	0.14	2035.70	0.14
Point 2	7052.60	6746.60	1228.43	0.22	2084.60	0.23
Point 3	7525.00	7219.00	1700.83	0.31	2172.80	0.32
Point 4	7996.40	7690.40	2172.23	0.39	2628.40	0.41
Point 5	8449.60	8143.60	2625.43	0.48	2939.40	0.49

(c) Calibration data for sensor 3

Soil + Container Weight (g)		Wet Weight (g)	Water Weight (g)	Gravimetric Water Content ($g\ g^{-1}$)	Sensor Measurements (RAW)	Volumetric Water Content ($m^3\ m^{-3}$)
Air dry	6997.40	6691.40	278.81	0.05	1938.20	0.05
Point 2	7478.60	7172.60	760.01	0.14	2018.20	0.14
Point 3	7952.00	7646.00	1233.41	0.23	2082.30	0.23
Point 4	8414.40	8108.40	1695.81	0.32	2324.80	0.32
Point 5	8872.20	8566.20	2153.61	0.41	2836.40	0.41

APPENDIX VI

Soil moisture data of the trench face for experimental setup 3

(a) Soil moisture data of the trench face at different depths on 31/07/2019

Time	Volumetric Moisture Content (%)		
	0 - 40 cm	40 - 80 cm	80 - 120 cm
00:00	38.17	31.71	40.33
01:00	38.20	31.72	40.37
02:00	38.22	31.72	40.38
03:00	38.21	31.74	40.38
04:00	38.20	31.74	40.39
05:00	38.20	31.74	40.39
06:00	38.21	31.76	40.39
07:00	38.23	31.75	40.44
08:00	38.20	31.77	40.40
09:00	38.20	31.75	40.40
10:00	38.19	31.74	40.40
11:00	38.16	31.73	40.36
12:00	38.13	31.71	40.36
13:00	38.13	31.68	40.34
14:00	38.02	31.65	40.27
15:00	38.02	31.63	40.29
16:00	38.00	31.63	40.31
17:00	37.97	31.63	40.31
18:00	37.98	31.62	40.31
19:00	38.01	31.63	40.34
20:00	38.00	31.62	40.31
21:00	38.02	31.63	40.32
22:00	38.02	31.65	40.32
23:00	38.01	31.65	40.32

(b) Soil moisture data of the trench face at different depths on 01/08/2019

Time	Volumetric Moisture Content (%)		
	0 - 40 cm	40 - 80 cm	80 - 120 cm
00:00	38.01	31.65	40.33
01:00	38.02	31.66	40.32
02:00	38.02	31.67	40.35
03:00	38.00	31.67	40.34
04:00	38.01	31.65	40.34
05:00	38.00	31.64	40.35
06:00	38.02	31.65	40.32
07:00	38.02	31.65	40.35
08:00	38.01	31.67	40.35
09:00	38.01	31.67	40.34
10:00	38.01	31.65	40.33
11:00	37.97	31.64	40.28
12:00	37.92	31.60	40.26
13:00	37.85	31.57	40.24
14:00	37.83	31.56	40.21
15:00	37.77	31.54	40.21
16:00	37.78	31.54	40.23
17:00	37.76	31.51	40.23
18:00	37.75	31.53	40.22
19:00	37.73	31.51	40.25
20:00	37.75	31.51	40.24
21:00	37.77	31.53	40.26
22:00	37.77	31.53	40.26
23:00	37.77	31.53	40.28

(c) Soil moisture data of the trench face at different depths on 02/08/2019

Time	Volumetric Moisture Content (%)		
	0 - 40 cm	40 - 80 cm	80 - 120 cm
00:00	37.77	31.54	40.25
01:00	37.78	31.54	40.25
02:00	37.76	31.56	40.26
03:00	37.78	31.55	40.28
04:00	37.79	31.57	40.26
05:00	37.78	31.56	40.26
06:00	37.77	31.57	40.26
07:00	37.79	31.56	40.25
08:00	37.78	31.58	40.28
09:00	37.79	31.56	40.25
10:00	37.77	31.55	40.27
11:00	37.74	31.54	40.25
12:00	37.69	31.52	40.22
13:00	37.69	31.51	40.21
14:00	37.67	31.51	40.20
15:00	37.66	31.49	40.21
16:00	37.62	31.48	40.20
17:00	37.61	31.47	40.18
18:00	37.59	31.46	40.20
19:00	37.61	31.46	40.21
20:00	37.62	31.46	40.21
21:00	37.62	31.46	40.22
22:00	37.62	31.47	40.23
23:00	37.62	31.47	40.21

(d) Soil moisture data of the trench face at different depths on 03/08/2019

Time	Volumetric Moisture Content (%)		
	0 - 40 cm	40 - 80 cm	80 - 120 cm
00:00	37.62	31.46	40.21
01:00	37.62	31.47	40.22
02:00	37.62	31.49	40.23
03:00	37.60	31.50	40.20
04:00	37.60	31.49	40.22
05:00	37.61	31.49	40.21
06:00	37.60	31.49	40.22
07:00	37.62	31.49	40.21
08:00	37.62	31.50	40.21
09:00	37.61	31.48	40.20
10:00	37.60	31.46	40.21
11:00	37.56	31.46	40.18
12:00	37.53	31.46	40.18
13:00	37.53	31.44	40.17
14:00	37.51	31.44	40.16
15:00	37.48	31.44	40.13
16:00	37.48	31.41	40.14
17:00	37.45	31.42	40.13
18:00	37.42	31.41	40.13
19:00	37.45	31.41	40.12
20:00	37.44	31.39	40.14
21:00	37.45	31.41	40.16
22:00	37.44	31.40	40.16
23:00	37.47	31.41	40.17

(e) Soil moisture data of the trench face at different depths on 04/08/2019

Time	Volumetric Moisture Content (%)		
	0 - 40 cm	40 - 80 cm	80 - 120 cm
00:00	37.48	31.41	40.15
01:00	37.47	31.41	40.15
02:00	37.48	31.41	40.16
03:00	37.47	31.41	40.16
04:00	37.48	31.41	40.20
05:00	37.47	31.41	40.16
06:00	37.47	31.42	40.16
07:00	37.48	31.41	40.17
08:00	37.48	31.43	40.14
09:00	37.47	31.41	40.14
10:00	37.47	31.40	40.14
11:00	37.44	31.40	40.14
12:00	37.43	31.41	40.12
13:00	37.41	31.41	40.12
14:00	37.39	31.40	40.09
15:00	37.34	31.39	40.10
16:00	37.34	31.37	40.08
17:00	37.33	31.36	40.08
18:00	37.30	31.36	40.08
19:00	37.29	31.36	40.09
20:00	37.29	31.34	40.07
21:00	37.31	31.34	40.09
22:00	37.30	31.33	40.09
23:00	37.31	31.34	40.10

(f) Soil moisture data of the trench face at different depths on 05/08/2019

Time	Volumetric Moisture Content (%)		
	0 - 40 cm	40 - 80 cm	80 - 120 cm
00:00	37.30	31.33	40.11
01:00	37.30	31.34	40.10
02:00	37.31	31.34	40.13
03:00	37.31	31.34	40.11
04:00	37.29	31.36	40.13
05:00	37.30	31.34	40.11
06:00	37.30	31.34	40.11
07:00	37.27	31.37	40.09
08:00	37.27	31.34	40.11
09:00	37.27	31.35	40.12
10:00	37.28	31.36	40.13
11:00	37.26	31.36	40.11
12:00	37.28	31.34	40.10
13:00	37.28	31.35	40.09
14:00	37.24	31.32	40.09
15:00	37.23	31.31	40.09
16:00	37.21	31.30	40.10
17:00	37.21	31.29	40.09
18:00	37.20	31.29	40.09
19:00	37.20	31.30	40.09
20:00	37.19	31.29	40.07
21:00	37.19	31.30	40.08
22:00	37.19	31.32	40.07
23:00	37.16	31.32	40.07

(g) Soil moisture data of the trench face at different depths on 06/08/2019

Time	Volumetric Moisture Content (%)		
	0 - 40 cm	40 - 80 cm	80 - 120 cm
00:00	37.17	31.32	40.07
01:00	37.17	31.32	40.07
02:00	37.18	31.32	40.09
03:00	37.19	31.30	40.09
04:00	37.19	31.32	40.07
05:00	37.18	31.31	40.09
06:00	37.17	31.31	40.11
07:00	37.18	31.31	40.11
08:00	37.17	31.32	40.13
09:00	37.19	31.31	40.10
10:00	37.20	31.30	40.12
11:00	37.19	31.34	40.10
12:00	37.14	31.31	40.09
13:00	37.17	31.31	40.08
14:00	37.17	31.30	40.07
15:00	37.22	31.27	40.09
16:00	37.37	31.28	40.08
17:00	41.10	31.58	40.34
18:00	41.32	36.80	41.24
19:00	41.46	36.98	41.76
20:00	42.04	38.76	43.14
21:00	41.90	38.19	43.19
22:00	41.66	37.29	43.02
23:00	41.56	36.72	42.86

(h) Soil moisture data of the trench face at different depths on 07/08/2019

Time	Volumetric Moisture Content (%)		
	0 - 40 cm	40 - 80 cm	80 - 120 cm
00:00	41.60	36.53	42.80
01:00	41.65	36.70	42.79
02:00	41.72	36.86	42.83
03:00	41.66	36.83	42.82
04:00	41.55	36.58	42.77
05:00	41.72	36.52	42.78
06:00	41.62	36.68	42.76
07:00	41.54	36.45	42.71
08:00	41.36	36.17	42.65
09:00	41.25	35.98	42.57
10:00	41.12	35.82	42.48
11:00	40.97	35.63	42.39
12:00	40.89	35.47	42.32
13:00	40.78	35.34	42.24
14:00	40.70	35.18	42.20
15:00	40.69	35.06	42.20
16:00	40.64	35.00	42.10
17:00	40.61	34.91	42.06
18:00	40.56	34.85	42.04
19:00	40.53	34.78	42.02
20:00	40.52	34.71	42.00
21:00	40.53	34.65	42.01
22:00	40.79	34.62	42.06
23:00	41.04	34.75	42.14

(i) Soil moisture data of the trench face at different depths on 08/08/2019

Time	Volumetric Moisture Content (%)		
	0 - 40 cm	40 - 80 cm	80 - 120 cm
00:00	41.13	35.07	42.19
01:00	41.19	35.42	42.20
02:00	41.12	35.56	42.22
03:00	41.06	35.51	42.23
04:00	41.01	35.43	42.24
05:00	40.99	35.35	42.19
06:00	40.92	35.30	42.18
07:00	40.85	35.21	42.14
08:00	40.84	35.12	42.10
09:00	40.76	35.03	42.08
10:00	40.73	34.97	42.04
11:00	40.70	34.88	42.00
12:00	40.67	34.76	41.97
13:00	40.72	34.71	42.12
14:00	41.02	34.84	42.20
15:00	41.17	35.17	42.20
16:00	41.72	36.24	42.29
17:00	41.79	36.93	42.53
18:00	41.70	36.76	42.77
19:00	41.57	36.46	42.76
20:00	41.55	36.19	42.67
21:00	41.94	36.51	42.77
22:00	42.34	37.79	43.21
23:00	42.63	38.94	43.54

(j) Soil moisture data of the trench face at different depths on 09/08/2019

Time	Volumetric Moisture Content (%)		
	0 - 40 cm	40 - 80 cm	80 - 120 cm
00:00	42.41	38.09	43.32
01:00	42.16	37.18	43.13
02:00	42.43	37.51	43.18
03:00	42.72	39.30	43.53
04:00	42.50	38.32	43.35
05:00	42.37	37.50	43.18
06:00	42.35	37.22	43.10
07:00	42.26	37.01	43.05
08:00	42.08	36.72	43.02
09:00	43.05	39.87	43.99
10:00	42.66	38.41	43.35
11:00	42.59	37.70	43.23
12:00	43.08	40.02	44.14
13:00	42.88	39.28	43.51
14:00	42.53	37.82	43.25
15:00	42.94	39.31	43.76
16:00	42.92	39.26	43.80
17:00	42.81	38.85	43.45
18:00	42.53	37.62	43.22
19:00	42.34	36.96	43.05
20:00	42.13	36.58	42.96
21:00	42.79	37.88	43.17
22:00	42.93	39.26	43.79
23:00	42.88	39.16	43.61

(k) Soil moisture data of the trench face at different depths on 10/08/2019

Time	Volumetric Moisture Content (%)		
	0 - 40 cm	40 - 80 cm	80 - 120 cm
00:00	42.79	38.71	43.40
01:00	42.53	37.56	43.22
02:00	42.35	36.96	43.07
03:00	42.43	36.71	43.12
04:00	42.92	38.93	43.58
05:00	42.74	38.28	43.38
06:00	42.53	37.36	43.19
07:00	42.30	36.81	43.06
08:00	42.11	36.50	42.97
09:00	42.24	36.27	43.05
10:00	42.95	39.59	43.79
11:00	43.00	39.54	43.86
12:00	42.95	39.47	43.86
13:00	42.84	38.85	43.40
14:00	42.57	37.50	43.19
15:00	42.92	38.57	43.36
16:00	42.78	38.54	43.38
17:00	42.57	37.42	43.19
18:00	42.39	36.87	43.05
19:00	42.11	36.49	42.95
20:00	42.13	36.27	42.86
21:00	42.32	36.51	42.88
22:00	42.47	36.76	43.05
23:00	43.12	39.61	44.11

(l) Soil moisture data of the trench face at different depths on 11/08/2019

Time	Volumetric Moisture Content (%)		
	0 - 40 cm	40 - 80 cm	80 - 120 cm
00:00	42.91	38.94	43.51
01:00	42.78	38.11	43.40
02:00	42.92	38.68	43.45
03:00	42.93	38.69	43.45
04:00	42.79	38.19	43.31
05:00	42.54	37.36	43.17
06:00	42.33	36.86	43.07
07:00	42.07	36.54	42.98
08:00	41.95	36.29	42.86
09:00	41.86	36.11	42.81
10:00	41.81	36.03	42.77
11:00	41.73	35.91	42.69
12:00	41.60	35.84	42.66
13:00	41.53	35.73	42.62
14:00	41.39	35.62	42.55
15:00	41.29	35.48	42.49
16:00	41.19	35.34	42.35
17:00	41.10	35.26	42.32
18:00	41.10	35.19	42.30
19:00	41.05	35.07	42.27
20:00	41.03	35.01	42.24
21:00	40.99	34.92	42.22
22:00	40.96	34.86	42.19
23:00	40.94	34.83	42.13

(m) Soil moisture data of the trench face at different depths on 12/08/2019

Time	Volumetric Moisture Content (%)		
	0 - 40 cm	40 - 80 cm	80 - 120 cm
00:00	40.90	34.76	42.08
01:00	40.86	34.68	42.05
02:00	40.85	34.63	42.03
03:00	40.80	34.60	42.00
04:00	40.78	34.57	42.00
05:00	40.74	34.56	41.98
06:00	40.75	34.50	41.96
07:00	40.74	34.50	41.94
08:00	40.70	34.47	41.92
09:00	40.67	34.43	41.88
10:00	40.63	34.38	41.87
11:00	40.60	34.38	41.84
12:00	40.55	34.32	41.80
13:00	40.46	34.27	41.75
14:00	40.35	34.18	41.70
15:00	40.35	34.16	41.71
16:00	40.33	34.12	41.70
17:00	40.32	34.09	41.70
18:00	40.27	34.04	41.68
19:00	40.27	34.00	41.67
20:00	40.27	33.98	41.67
21:00	40.23	33.98	41.68
22:00	40.23	33.96	41.65
23:00	40.21	33.92	41.65

(n) Soil moisture data of the trench face at different depths on 13/08/2019

Time	Volumetric Moisture Content (%)		
	0 - 40 cm	40 - 80 cm	80 - 120 cm
00:00	40.22	33.93	41.65
01:00	40.23	33.90	41.65
02:00	40.21	33.85	41.82
03:00	41.62	34.14	42.42
04:00	42.05	36.84	42.33
05:00	42.17	37.28	42.90
06:00	42.49	38.23	43.25
07:00	42.30	37.49	43.22
08:00	42.14	36.93	43.10
09:00	41.96	36.56	42.98
10:00	41.81	36.25	42.87
11:00	41.60	36.01	42.76
12:00	41.50	35.81	42.63
13:00	41.33	35.65	42.54
14:00	41.21	35.45	42.44
15:00	41.10	35.27	42.41
16:00	41.04	35.16	42.25
17:00	41.00	35.07	42.20
18:00	40.96	34.95	42.32
19:00	41.68	35.46	42.43
20:00	41.75	36.05	42.39
21:00	41.71	36.22	42.44
22:00	41.63	36.15	42.55
23:00	41.57	36.06	42.58

(o) Soil moisture data of the trench face at different depths on 14/08/2019

Time	Volumetric Moisture Content (%)		
	0 - 40 cm	40 - 80 cm	80 - 120 cm
00:00	41.50	35.94	42.56
01:00	41.43	35.81	42.53
02:00	41.32	35.63	42.48
03:00	42.19	36.15	42.67
04:00	42.73	38.58	43.48
05:00	42.77	38.35	43.40
06:00	42.52	37.51	43.21
07:00	42.38	37.05	43.06
08:00	42.22	36.69	42.99
09:00	42.43	37.01	43.11
10:00	42.64	38.17	43.27
11:00	42.39	37.43	43.17
12:00	42.20	36.89	43.03
13:00	41.99	36.51	42.89
14:00	41.81	36.20	42.75
15:00	41.62	35.97	42.68
16:00	41.53	35.79	42.58
17:00	41.37	35.57	42.48
18:00	41.32	35.42	42.44
19:00	41.26	35.33	42.38
20:00	41.19	35.23	42.34
21:00	41.13	35.17	42.31
22:00	41.12	35.09	42.27
23:00	41.05	35.01	42.24

APPENDIX VII

Soil moisture study analysis for the trench face for experimental setup 3

Date	Depth (cm)	Time	Volumetric Moisture Content (%)	Increase in Volumetric Moisture Content (%)	Discharge (l)	Total Discharge (l)	
06-08-2019	0 - 40	14:00	38.14	3.90	31.20	31.20	100.00
		20:00:0	42.04				
	40 - 80	15:00	32.27	6.49	51.92	51.92	
		20:00	38.76				
	80 - 120	16:00	41.08	2.11	16.88	16.88	
		21:00	43.19				
08-08-2019	0 - 40	12:00	40.76	1.03	8.24	16.88	62.00
		17:00	41.79				
		20:00	41.55	1.08	8.64		
		23:00	42.63				
	40 - 80	13:00	35.71	1.22	9.76	31.76	
		17:00	36.93				
		20:00	36.19	2.75	22.00		
		23:00	38.94				
	80 - 120	12:00	41.97	0.80	6.40	13.36	
		18:00	42.77				
		20:00	42.67	0.87	6.96		
		23:00	43.54				
09-08-2019	0 - 40	01:00	42.16	0.56	4.48	25.84	133.92
		03:00	42.72				
		08:00	42.08	0.97	7.76		
		09:00	43.05				
		11:00	42.59	0.49	3.92		
		12:00	43.08				
		14:00	42.53	0.41	3.28		
		15:00	42.94				
		20:00	42.13	0.80	6.40		
		22:00	42.93				
	40 - 80	01:00	38.09	1.21	9.68	78.80	
		03:00	39.30				
		08:00	37.72	2.15	17.20		
		09:00	39.87				
		11:00	37.70	2.32	18.56		

		12:00	40.02				
		14:00	37.82	1.49	11.92		
		15:00	39.31				
		20:00	36.58	2.68	21.44		
		22:00	39.26				
		01:00	43.13	0.40	3.20		
		03:00	43.53				
		08:00	43.02	0.97	7.76		
	80 - 120	09:00	43.99				
		11:00	43.23	0.91	7.28	29.28	
		12:00	44.14				
		14:00	43.25	0.55	4.40		
		16:00	43.80				
		20:00	42.96	0.83	6.64		
		22:00	43.79				
		02:00	42.35	0.57	4.56		
		04:00	42.92				
		08:00	42.11	0.89	7.12		
	0 - 40	11:00	43.00			22.96	
		14:00	42.57	0.40	3.20		
		15:00	42.97				
		19:00	42.11	1.01	8.08		
		23:00	43.12				
		03:00	36.71	2.22	17.76		
		04:00	38.93				
		09:00	37.27	2.32	18.56		
10-08-2019	**40 - 80**	10:00	39.59			63.60	109.28
		14:00	37.50	1.07	8.56		
		15:00	38.57				
		20:00	37.27	2.34	18.72		
		23:00	39.61				
		02:00	43.07	0.51	4.08		
		04:00	43.58				
		08:00	42.97	0.89	7.12		
	80 - 120	11:00	43.86			22.72	
		14:00	43.19	0.19	1.52		
		16:00	43.38				
		20:00	42.86	1.25	10.00		
		23:00	44.11				
	0 - 40	01:00	42.78	0.15	1.20	1.20	
		03:00	42.93				6.24
11-08-2019	**40 - 80**	01:00	38.11	0.58	4.64	4.64	
		03:00	38.69				

	80 - 120	01:00	43.40	0.05	0.40	0.40	
		03:00	43.45				
13-08-2019	**0 - 40**	02:00	40.21	2.28	18.24	24.56	77.60
		06:00	42.49				
		18:00	40.96	0.79	6.32		
		20:00	41.75				
	40 - 80	02:00	34.85	3.38	27.04	37.20	
		06:00	38.23				
		18:00	34.95	1.27	10.16		
		21:00	36.22				
	80 - 120	01:00	41.65	1.60	12.80	15.84	
		06:00	43.25				
		17:00	42.20	0.38	3.04		
		23:00	42.58				
14-08-2019	**0 - 40**	02:00	41.32	1.45	11.60	14.96	52.64
		05:00	42.77				
		08:00	42.22	0.42	3.36		
		10:00	42.64				
	40 - 80	02:00	36.63	1.95	15.60	27.44	
		04:00	38.58				
		08:00	36.69	1.48	11.84		
		10:00:00	38.17				
	80 - 120	02:00:00	42.48	1.00	8.00	10.24	
		04:00:00	43.48				
		08:00:00	42.99	0.28	2.24		
		10:00:00	43.27				

DETERMINATION OF SUBSURFACE STORMFLOW USING TRACER METHOD

By

ADARSH S S

(2017-18-008)

Abstract

Submitted in partial fulfillment of the requirement for the degree of

Master of Technology

In

Agricultural Engineering

(Soil and Water Engineering)

Faculty of Agricultural Engineering and Technology

Kerala Agricultural University

Department of Soil and Water Conservation Engineering

KELAPPAJI COLLEGE OF AGRICULTURAL ENGINEERING AND TECHNOLOGY

TAVANUR-679573, MALAPPURAM

KERALA, INDIA

2020

ABSTRACT

The state of Kerala in India is a typical example of a region facing droughts of varying degrees despite receiving high annual rainfall. This is because a lion share of the precipitation received is going out as runoff without recharging the groundwater. The subsurface stormflow is considered as the fast moving component of subsurface runoff on which very little information is available due to its complex mechanism of movement through subsurface. Hence, this study has been taken up for gathering more knowledge on the phenomenon of subsurface stormflow with the help of monitoring of soil moisture movement and tracer method. For data collection, three experimental setups in two experimental plots have been setup in KCAET campus, Kerala, India. It is a lateritic terrain having sandy loam type of soil and a general slope. Through-flow trenches were constructed for all the three setups and studied the soil moisture variation on the trench face at three depths (0-40 cm, 40-80 cm and 80-120 cm) in order to study the subsurface stormflow through different depths. For the experimental setup 1, simulation of rainfall was done using a butterfly sprinkler as the input. Line application of water was done for the experimental setup 2. Natural rain was taken as the input for the experimental setup 3. The subsurface stormflow through the soil matrix is also studied by the salt tracer experiment for obtaining its velocities. From the study it was found that the subsurface stormflow discharge is greatly affected by the soil dry density and soil suction. The subsurface stormflow discharge was found to have negative correlations with both soil suction and soil dry density. The subsurface stormflow velocities through 0-40 cm, 40-80 cm and 80-120 cm depths obtained from the soil moisture variation studies were 23.74 cm day^{-1}, 36.23 cm day^{-1} and 17.41 cm day^{-1} respectively and the same obtained through the tracer studies were 27.27 cm day^{-1}, 30 cm day^{-1} and 26.67 cm day^{-1} respectively. It was also concluded that the prevailing subsurface stormflow in the experimental sites is due to matrix flow rather than the preferential flow. The results gave the conclusion that high value of rainfall along with low values of soil dry density and soil suction can induce the subsurface stormflow even in the area having gentle slope (<10 %).